

**GRAESERITE, $\text{Fe}_4\text{Ti}_3\text{AsO}_{13}(\text{OH})$,
A NEW MINERAL SPECIES OF THE DERBYLITE GROUP FROM THE
MONTE LEONE NAPPE, BINNTAL REGION, WESTERN ALPS, SWITZERLAND**

MICHAEL S. KRZEMNICKI¹

*Mineralogisch-Petrographisches Institut, Universität Basel, Bernoullistr. 30, CH-4056 Basel,
Switzerland*

ERIC REUSSER¹

Institut für Mineralogie und Petrographie, ETH-Zentrum, Sonneggstr. 5, CH-8092 Zurich, Switzerland

ABSTRACT

Graeserite, ideally $\text{Fe}_4\text{Ti}_3\text{AsO}_{13}(\text{OH})$, is a new mineral species of the derbylite group, which includes derbylite, tomichite, and hemloite. It is found in needle-shaped crystals, elongate along the *c* axis. Graeserite is monoclinic, space group *A2/m*, with the cell parameters *a* 7.184(2), *b* 14.289(6), *c* 5.006(2) Å, β 105.17(2)°, *V* 495.9(2) Å³, *Z* = 2, *D*_{calc.} = 4.56 g/cm³. The VHN_{25g} is 521 (Mohs hardness ~5½). The strongest five lines of the X-ray powder-diffraction pattern [*d* in Å(*I*)(*hkl*)] are: 2.681(100)($\bar{2}$ 31), 2.846(80)(131), 1.583(50)(351), 3.117 (30)(220), and 2.029(30)(122). Graeserite is black and metallic, with a black streak; it displays a conchoidal fracture. Pleochroism, bireflectance and internal reflections were not observed. The measured values of reflectance in air are compared with those of other members of the derbylite group. Electron-microprobe analyses gave TiO₂ 40.89, Fe₂O₃ 33.64, FeO_{calc.} 3.94, PbO 5.00, As₂O₃ 13.51, Sb₂O₃ 1.43, and H₂O_{calc.} 1.30, total 99.80 wt.%. The empirical formula, based on 13 atoms of oxygen and one hydroxyl group, is (Fe³⁺_{2.91}Fe²⁺_{0.38}Ti_{0.54}Pb_{0.15}) Σ _{3.98}Ti₃(As³⁺_{0.94}Sb³⁺_{0.07}) Σ _{1.01}O₁₃(OH). Graeserite occurs as a hydrothermal mineral in Alpine-type fissures in gneisses of the Monte Leone nappe at the locality Lärcheltini, in the Binntal region of Switzerland, in association with other rare arsenic oxides. With the name, we honor Stephan Graeser, University of Basel, Switzerland, for his fundamental studies of arsenic-bearing minerals.

Keywords: graeserite, new mineral species, derbylite group, Binntal region, Western Alps, Switzerland.

SOMMAIRE

La graeserite, de composition idéale $\text{Fe}_4\text{Ti}_3\text{AsO}_{13}(\text{OH})$, est une nouvelle espèce minérale du groupe de la derbylite, qui inclut derbylite, tomichite, et hemloite. Elle se présente en cristaux aciculaires allongés selon l'axe *c*. La graeserite est monoclinique, groupe spatial *A2/m*, paramètres réticulaires *a* 7.184(2), *b* 14.289(6), *c* 5.006(2) Å, β 105.17(2)°, *V* 495.9(2) Å³, *Z* = 2, *D*_{calc.} = 4.56 g/cm³. La dureté VHN_{25g} est de 521 (~5½ sur l'échelle de Mohs). Les cinq raies les plus intenses du spectre de diffraction X (méthode des poudres) [*d* en Å(*I*)(*hkl*)] sont: 2.681(100)($\bar{2}$ 31), 2.846(80)(131), 1.583(50)(351), 3.117 (30)(220), et 2.029(30)(122). La graeserite est noir métallique, avec une rayure noire; elle possède une fracture conchoïdale. Nous avons décelé ni pléochroïsme, ni biréflectance, ni réflexions internes. Les valeurs mesurées de réflectance dans l'air sont comparées avec celles d'autres membres du groupe de la derbylite. Les analyses obtenues par microsonde électronique ont donné TiO₂ 40.89, Fe₂O₃ 33.64, FeO_{calc.} 3.94, PbO 5.00, As₂O₃ 13.51, Sb₂O₃ 1.43, et H₂O_{calc.} 1.30, total 99.80% (par poids). La formule empirique, calculée sur une base de 13 atomes d'oxygène et un groupe d'hydroxyle, est (Fe³⁺_{2.91}Fe²⁺_{0.38}Ti_{0.54}Pb_{0.15}) Σ _{3.98}Ti₃(As³⁺_{0.94}Sb³⁺_{0.07}) Σ _{1.01}O₁₃(OH). La graeserite est le produit d'une cristallisation hydrothermale dans des fentes alpines dans des gneiss de la nappe de Monte Leone à Lärcheltini, dans la région de Binntal, en Suisse; elle y est associée à d'autres oxydes d'arsenic rares. Par le choix du nom, nous honorons Stefan Graeser, de l'Université de Bâle, en Suisse, qui a fait des études fondamentales des minéraux d'arsenic.

(Traduit par la Rédaction)

Mots-clés: graeserite, nouvelle espèce minérale, groupe de la derbylite, région de Binntal, Alpes occidentales, Suisse.

¹ E-mail addresses: haennih@ubaclu.unibas.ch, eric@erdw.ethz.ch

INTRODUCTION

Graeserite, ideally $\text{Fe}_4\text{Ti}_3\text{AsO}_{13}(\text{OH})$, is a new mineral species found in Alpine-type fissures in paragneisses of the Monte Leone nappe, Binntal region, Western Alps, Switzerland. It belongs to the derbylite group, which consists of the species derbylite, tomichite (including barian tomichite), and hemloite (Table 1). Except for hemloite, the minerals of this group exhibit the general formula $M^{3+}_xM^{4+}_y\text{O}_{13}(\text{OH})$. The cation site M^{3+} is occupied by Fe^{3+} and V^{3+} (with occasionally some Fe^{2+} , Pb^{2+} , and Ti^{4+}), and the M^{4+} site by Ti^{4+} . Both the M^{3+} and M^{4+} sites are octahedrally coordinated. The tetrahedrally coordinated T site is occupied by Sb^{3+} , As^{3+} , and occasionally Ba^{2+} in barian tomichite. The values for the stoichiometric coefficients $x:y$ are commonly 4:3 (derbylite, tomichite, and graeserite), but may also amount to 5:2 (barian tomichite).

Derbylite was discovered a century ago (Hussak & Prior 1897) in cinnabar-bearing gravels at Tripuhy, Minas Gerais, Brazil. Its close-packed oxide crystal structure was determined by Moore & Araki (1976) and refined by Mellini *et al.* (1983). Tomichite was first reported by Nickel & Grey (1979) from the Kalgoorlie gold deposit in Australia. The crystal structure of tomichite was determined by Grey *et al.* (1987), who further reported barian tomichite at the Hemlo gold deposit, Ontario. From the same deposit, Harris *et al.* (1989) described hemloite as a further member of the derbylite group.

In this study, we present mineralogical, chemical and preliminary structural data for graeserite. Graeserite is named in honor of Professor Stefan Graeser (b. 1935), of the Mineralogical–Petrographic Institute, University of Basel, Switzerland, who has been involved for years in research on oxides and sulfosalts of arsenic in the Binntal region of the Monte Leone nappe (Graeser 1966, Graeser & Roggiani 1976, Graeser *et al.* 1994, and references therein). Both the mineral and the name have been approved by the IMA Commission on New Minerals and Mineral Names (proposal 96–010). Specimens are held at the Natural History Museum in Basel, Switzerland.

OCCURRENCE

Graeserite was discovered 1995 in hydrothermal veins that occur in a two-mica paragneiss of the Monte Leone nappe, Binntal region, Western Alps, Switzerland, or in small cavities in proximity to such veins (wallrock alteration). Numerous specimens have been found at the locality Lärcheltini (Fig. 1), accompanied by a wide range of other hydrothermal minerals, including anatase, arsenopyrite, asbescasite, bournonite, cafarsite, cervandonite-(Ce), chernovite, fetiasite, gold (traces), hematite, magnetite, monazite-(Ce), rutile and tennantite.

The formation of graeserite is attributed to the hydrothermal activity associated with the Tertiary Alpine

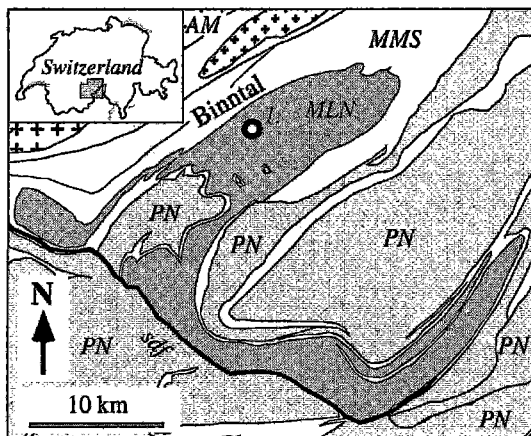


FIG. 1. General tectonic map of the Binntal region, Western Alps, Switzerland. Symbols: *l.* locality Lärcheltini, *MLN* Monte Leone nappe, *PN* Penninic nappes, *MMS* Mesozoic metasediments, *AM* Aar massif (granites), *sdf* Simplicon detachment fault.

orogeny, which affected the whole Alpine region by extensive ductile–brittle deformations and regional metamorphism reaching conditions of the lower amphibolite facies in the Monte Leone nappe. The regional geology is discussed in more detail by Streckeisen *et al.* (1974), Steck (1987), Hügi (1988), and Krzewnicky (1996). Several Prealpine ore concentrations (As–Fe–Cu–Pb sulfides) within this nappe were locally remobilized, thus generating some unique hydrothermal mineralizations (*e.g.*, Lengenbach, Pizzo Cervandone, Wannigletscher, Lärcheltini; *cf.* Graeser 1966, Graeser & Roggiani 1976, Krzewnicky 1996).

PHYSICAL AND OPTICAL PROPERTIES

Table 2 presents a summary of the physical properties of graeserite compared with the other members of the derbylite group. Graeserite, monoclinic *A2/m*, is generally found in well-developed, euhedral crystals that are elongate along the *c* axis. Commonly, they are needle-shaped (<10 μm thick, up to 5 mm long, Fig. 2). Lineations parallel to the *c* axis indicate extensive twinning. Occasionally, graeserite occurs in radial aggre-

TABLE 1. MINERALS OF THE DERBYLITE GROUP

Mineral	Chemical Formula	Space Group
Derbylite	$\text{Fe}_4\text{Ti}_3\text{SbO}_{13}(\text{OH})$	<i>P2₁/m</i>
Tomichite	$(\text{V,Fe})_4\text{Ti}_3\text{AsO}_{13}(\text{OH})$	<i>P2₁/m</i>
Barian Tomichite	$(\text{V,Fe})_4\text{Ti}_3\text{Ba}_{0.5}(\text{As})_{0.5}\text{O}_{13}(\text{OH})$	<i>A2/m</i>
Graeserite	$\text{Fe}_4\text{Ti}_3\text{AsO}_{13}(\text{OH})$	<i>A2/m</i>
Hemloite	$(\text{Ti,V,Fe,Al})_{12}(\text{As,Sb})_2\text{O}_{23}$	<i>PI</i>

TABLE 2. COMPARISON OF THE DERBYLITE-GROUP MINERALS

	Graeserite	Tomichite	Barian tomichite	Derbylite
System	monoclinic	monoclinic	monoclinic	monoclinic
Space group	<i>A2/m</i>	<i>P2₁/m</i>	<i>A2/m</i>	<i>P2₁/m</i>
<i>a</i> (Å)	7.184	7.119	7.105	7.16
<i>b</i> (Å)	14.289	14.176	14.21	14.347
<i>c</i> (Å)	5.006	4.992	5.043	4.97
β (°)	105.17	105.05	104.97	104.61
<i>V</i> (Å ³)	495.9			
<i>D</i> _{calc} (g/cm ³)	4.56	4.42		4.76
microhardness				
VHN ₂₅	521	800		
color	opaque, black	opaque, black	opaque, black	resinous, black
color values	<i>R1 R2</i>	<i>R1 R2</i>		<i>R1 R2</i>
<i>x</i>	0.300 0.300	0.311 0.312		0.298 0.298
<i>y</i>	0.305 0.305	0.316 0.317		0.303 0.302
<i>Y</i> %	18.6 17.5	17.1 17.8		18 19.1
λ	476 476	504 589		476 475
<i>P e</i> %	5.2 5.2	0.3 0.7		5.9 6.2
type locality	Lärcheltini Binntal Switzerland	Kalgoorlie Western Australia	Hemlo deposit Ontario	Tripuhy Minas Gerais Brazil

TABLE 3. GRAESERITE: REFLECTED-LIGHT MICROSCOPY

λ	reflectance values			color values C illuminant	
	<i>R1</i>	<i>R2</i>		<i>R1</i>	<i>R2</i>
400 nm	22.6 %	23.5 %	<i>x</i>	0.2997	0.2998
420	21.7	22.5			
440	20.9	21.6	<i>y</i>	0.3049	0.3048
460	20.1	20.8			
480	19.6	20.3	<i>Y</i> %	18.6	17.5
500	19.3	19.9			
520	19.0	19.6			
540	18.7	19.3			
560	18.4	19.0	<i>1 d</i>	476.4	475.9
580	18.2	18.9			
600	18.1	18.6	<i>P e</i> %	5.2	5.2
620	17.9	18.5			
640	17.7	18.3			
660	17.5	18.1			
680	17.3	17.9			
700	17.3	17.9			

gates, which are attached to fetiasite and in some cases intergrown with feldspar crystals.

Graeserite displays a distinct ductile behavior; thus the crystals commonly are deformed and curved during sample preparation. Therefore, it is rather difficult to investigate the morphology by optical goniometer or to determine the crystal structure of graeserite by single-crystal X-ray methods. Graeserite exhibits a moderate cleavage along {100} and a conchoidal fracture. The density could not be measured directly by immersion in heavy liquids, as it is greater than that of Clerici solution, but was calculated on the basis of the empirical formula; *Dx* 4.56 g/cm³. The Vickers hardness was

measured with a load of 25 g on a polished section of a graeserite aggregate. The mean value of VHN₂₅, 521, corresponds to a Mohs hardness of about 5½.

For reflectance measurements, we used a Leitz microscope with a Zeiss-SiC reference standard. Data measured in air only are listed in Table 3. A comparison of the data with values for derbylite and tomichite reveals a close similarity between graeserite and derbylite (Fig. 3). Pleochroism, bireflectance and internal reflections were not observed. The optical data are given in Table 2.

Raman spectra were obtained on a Renishaw Raman system 1000 (Swiss Gemmological Institute SSEF,

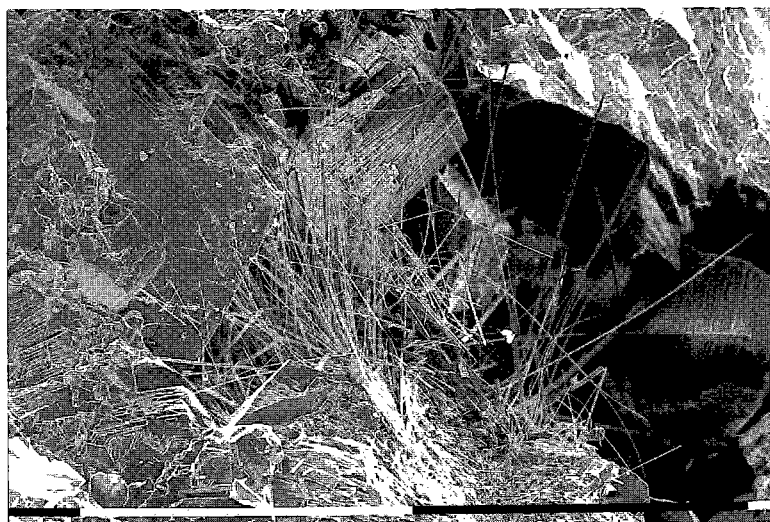


FIG. 2. SEM photomicrograph of an aggregate of graeserite crystals. Scale bar: 1 mm.

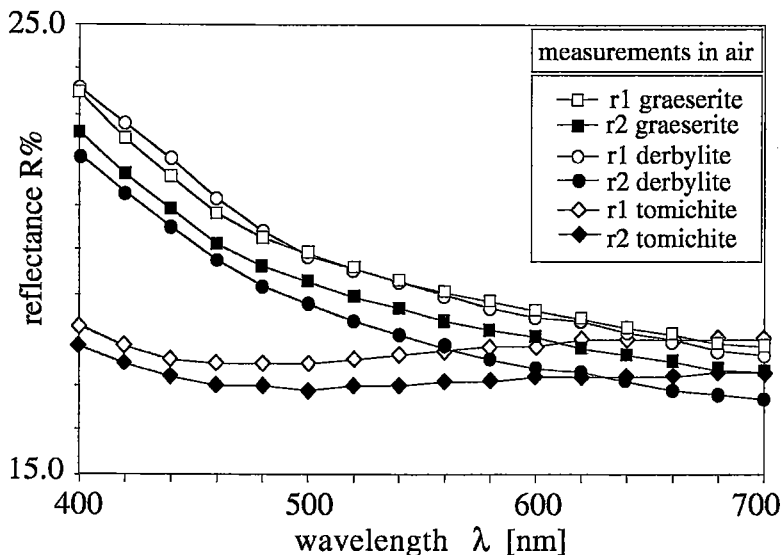


FIG. 3. Comparison of reflectance data for the derbylite-group minerals. The reflectance values $R\%$ versus wavelength λ [nm] diagram (measured in air) reveals a close similarity between graeserite and derbylite.

Basel) with an argon laser (25 mW, omnichrome). A typical spectrum for graeserite is shown in Figure 4, as it may aid in identification.

X-RAY CRYSTALLOGRAPHY AND CHEMICAL COMPOSITION

X-ray-diffraction analyses by precession and Weissenberg techniques showed graeserite to be monoclinic $A2/m$. The cell parameters were refined from powder data and are compared with those of the other members of the derbylite group (Table 2). The indexed X-ray powder-diffraction data for graeserite are listed in Table 4. There are strong similarities between the powder pattern of graeserite and those of other derbylite-group minerals, which point to a close structural relationship among this group of minerals (Nickel & Grey 1979, Mellini *et al.* 1983, Grey *et al.* 1987, Berlepsch & Armbruster 1998).

All samples of graeserite were first analyzed qualitatively by energy-dispersion spectroscopy (ED-XRF) for element identification. These analyses and photographic documentation were carried out with a Philips 515 scanning electron microscope, equipped with an ED-XRF spectrometer (SEM Laboratory, University of Basel).

Six samples were analyzed quantitatively using a Cameca SX-50 electron microprobe with an acceleration voltage of 20 kV and a beam current of 10 nA. The following elements were measured (standards in parentheses): Fe (hematite), Ti (rutile), Mn (spessartine), Pb (galena), Si (quartz), As (synthetic GaAs), and Sb (syn-

thetic Sb_2O_3). Vanadium and barium, which are important constituents of tomichite and barian tomichite, were found to be below the limit of detection. All data were corrected for matrix effects by a ZAF-type online procedure. The average composition determined from results of 39 analyses (6 samples) is shown in Table 5. The chemical composition of all the samples is rather uniform, although the concentrations of Fe, Ti, Pb and Sb show some variation from sample to sample. Back-scattered-electron images (BSE) revealed no compositional zoning within the analyzed samples.

The normalization of the graeserite formula (Table 5) is based on a total of 27 negative charges (*i.e.*, $O^{2-}_{13} + OH^-$) and a sum of eight cations at the M^{3+} , M^{4+} , and T sites, as first proposed by Moore & Araki (1976) for derbylite. The H_2O content was calculated assuming one hydroxyl group per formula unit (Moore & Araki 1976). According to Grey *et al.* (1987) and Mellini *et al.* (1983), charge balance is usually maintained by variation in the ratio of Fe^{2+} to Fe^{3+} . In graeserite, this ratio (~ 0.130) is comparable with the one found in derbylite ($Fe^{2+}/Fe^{3+} \approx 0.155$; Mellini *et al.* 1983). The similarity in the values may be interpreted as a further indication of a close structural relationship between these two minerals.

The empirical formula for graeserite, derived from electron-microprobe data (based on the average results, Table 5), is $(Fe^{3+}_{2.91}Fe^{2+}_{0.38}Ti_{0.54}Pb_{0.15})_{\Sigma 3.98}Ti_3(As^{3+}_{0.94}Sb^{3+}_{0.07})_{\Sigma 1.01}O_{13}(OH)$, which is in good agreement with the composition $Pb_{0.14}(Fe,Ti)_7AsO_{12+x}(OH)_{2-x}$ obtained from the structure determination (Berlepsch & Armbruster 1998) on material from the

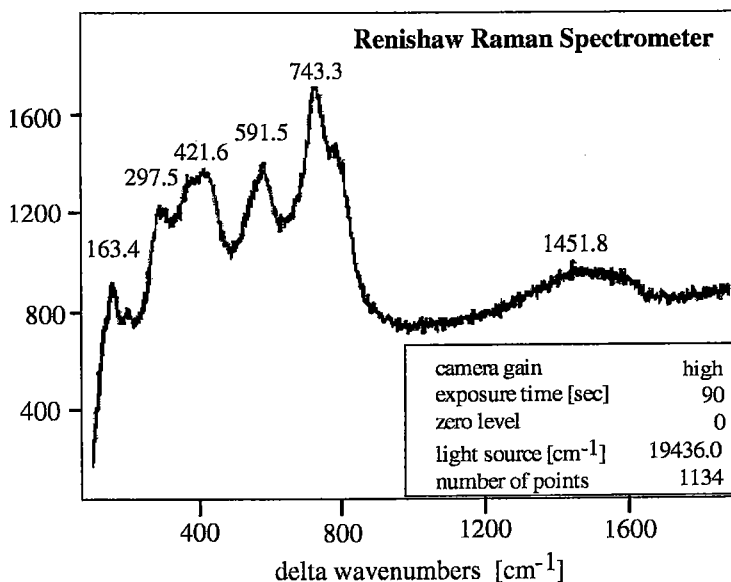


FIG. 4. Raman spectrum of graeserite, as obtained with a Renishaw Raman spectrometer.

same locality. The idealized formula of graeserite may be written as $Fe_4Ti_3AsO_{13}(OH)$. The analyzed samples all contain some Pb^{2+} and Fe^{2+} (calculated on the basis of charge balance) and a small excess in Ti^{4+} with respect to the idealized stoichiometry. The incorporation of these substituting elements is probably due to the heterovalent substitution [i] $(Fe, Pb)^{2+}Ti^{4+}$ at the M^{3+} site. A plot (Fig. 5) of amount of Fe^{3+} versus $\Sigma(Fe,Pb)^{2+} + Ti^{4+}$ reveals a distinct negative correlation (slope: -1.043 , $R^2 = 0.924$), which fits well with this mechanism of substitution. A bivariate plot for As^{3+} versus Sb^{3+} exhibits only a weak negative correlation, although the incorporation of minor Sb in graeserite is easily explained by a simple exchange substitution between Sb^{3+} and As^{3+} at the arsenic site.

TABLE 4. X-RAY-DIFFRACTION DATA FOR GRAESERITE

I_{rel}	d_{obs}	d_{calc}	<i>hkl</i>	I_{rel}	d_{obs}	d_{calc}	<i>hkl</i>
30	3.117	3.119	220	20	1.7234	1.7235	222
80	2.846	2.847	131	20	1.6218	1.6224	213
100	2.681	2.683	231			1.5834	422
20	2.495	2.493	102	50	1.5825	1.5824	351
20	2.225	2.226	151			1.5816	162
20	2.148	2.145	251	20	1.5150	1.5151	451
30	2.029	2.029	122			1.4405	153
20	1.8093	1.8088	351	10	1.4400	1.4400	431
20	1.7765	1.7760	202			1.3661	413
				20	1.3647	1.3648	182

Powder data with Debye-Scherrer camera, $FeK\alpha$ radiation. Intensities I_{rel} by visual estimation; d_{obs} determined from the cell parameters a 7.184, b 14.289, c 5.006 Å, β 105.17°. Values of d_{obs} and d_{calc} are expressed in Å.

DISCUSSION

Derbylite, tomichite, barian tomichite, hemloite, and graeserite are rare accessory phases known to date from only a few deposits worldwide: Tripuhy (Brazil), Kalgoorlie (Australia), Hemlo (Ontario, Canada), Buca della Vena (Italy), and Lärcheltini (Switzerland). The complex mineralizations of these deposits are commonly attributed to metasomatic and hydrothermal fluids (Mellini *et al.* 1983, Grey *et al.* 1987, Graeser & Roggiani 1976). Graeserite, as well as the other

TABLE 5. CHEMICAL COMPOSITION OF GRAESERITE

	mean wt%	range	1 σ	<i>apfu</i>	
TiO ₂	40.89	(39.75 - 41.92)	0.46	Ti ⁴⁺	3.54
Fe ₂ O ₃	33.64	(31.65 - 35.55)	0.85	Fe ³⁺	2.91*
FeO	3.94	(3.20 - 4.85)	0.43	Fe ²⁺	0.38*
PbO	5.00	(2.22 - 6.35)	1.05	Pb ²⁺	0.15
MnO	0.06	(n.d. - 0.13)	0.03	Mn ²⁺	0.01
As ₂ O ₃	13.51	(13.12 - 14.31)	0.30	As ³⁺	0.94
Sb ₂ O ₃	1.43	(0.7 - 2.33)	0.45	Sb ³⁺	0.07
SiO ₂	0.02	(n.d. - 0.08)	0.02	Si ⁴⁺	0.00
H ₂ O	1.30	(1.28 - 1.34)	0.01	OH ⁻	1.00*
Total	99.79				

Electron-microprobe data, reported in wt%. The range of 39 analyses is reported. The normalization is based on 8 cations per formula unit and a total of 27 negative charges. The proportion of Fe³⁺ and Fe²⁺ was calculated based on charge-balance constraints. The FeO and Fe₂O₃ contents were recalculated, on the basis of the Fe³⁺/Fe²⁺ ratio. The proportion of H₂O was determined on the assumption of one hydroxyl group per formula unit (*cf.* Moore & Araki 1976, Grey *et al.* 1987, Mellini *et al.* 1983). n.d.: not detected (below the limit of detection limit); *apfu*: atoms per formula unit. The concentration of V and Ba are invariably below the limit of detection.

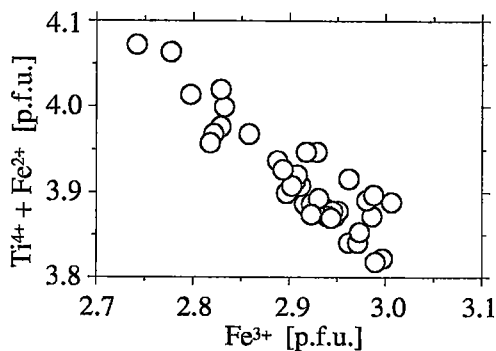


FIG. 5. A plot of the concentration of Fe^{3+} versus $\Sigma(\text{Fe}, \text{Pb})^{2+} + \text{Ti}^{4+}$ reveals a distinct negative correlation, which fits very well the proposed mechanism of heterovalent substitution [i] $(\text{Fe}, \text{Pb})^{2+}\text{Ti}^{4+}\text{Fe}^{3+}_{-2}$. [pfu]: per formula unit.

members of the derbylite group, seem to be related to the presence of Au mineralization (e.g., tomichite: Kalgoorlie gold deposit; barian tomichite: Hemlo gold deposit, hemloite: Hemlo gold deposit). At Lärcheltini, the occurrence of native gold (traces) close to graeserite has recently been confirmed (T. Mumenthaler, pers. commun.).

Finally, it seems likely that an isomorphic series (partial or even complete) exists between graeserite and both derbylite and tomichite. This conclusion is based on the proposed mechanism of substitution on various sites in graeserite, and in addition on structural and crystallographic analogies between these minerals (e.g., Tables 2, 3).

ACKNOWLEDGEMENTS

The authors thank R. Guggenheim and D. Mathys (SEM Laboratory, Basel) for their valuable contribution to this study. Raman spectra investigations were kindly provided by H.A. Hänni (Swiss Gemmological Institute SSEF, Basel); the assistance of M. Doppler (University of Geneva, Switzerland) for the ore-microscopy measurements is appreciated. We acknowledge the fruitful discussions with R. Gieré, J. Brugger and P. Berlepsch. Thanks also to T. Mumenthaler and R. Lüssi, who kindly provided some samples of graeserite. This study was financially supported by the Swiss National Science Foundation (grants No. 21-33830.92 and 20-40603.94). Reviews by P.B. Leavens and an anonymous referee are gratefully acknowledged.

REFERENCES

BERLEPSCH, P. & ARMBRUSTER, T. (1998): The crystal structure of Pb^{2+} -bearing graeserite, $\text{Pb}_{0.14}(\text{Fe}, \text{Ti})_7\text{AsO}_{12+x}(\text{OH})_{2-x}$, a mineral of the derbylite group. *Schweiz. Mineral. Petrogr. Mitt.* **78**, 1-9.

GRAESER, S. (1966): Asbecasit und Cafarsit, zwei neue Mineralien aus dem Binnatal (Kt. Wallis). *Schweiz. Mineral. Petrogr. Mitt.* **46**, 367-375.

_____ & ROGGIANI, A.G. (1976): Occurrence and genesis of rare arsenate and phosphate minerals around Pizzo Cervandone, Italy/Switzerland. *Rend. Soc. Ital. Mineral. Petrogr.* **32**, 279-288.

_____, SCHWANDER, H., DEMARTIN, F., GRAMACCIOLI, C.M., PILATI, T. & REUSSER, E. (1994): Fetiasite $(\text{Fe}^{2+}, \text{Fe}^{3+}, \text{Ti})_3\text{O}_2[\text{As}_2\text{O}_5]$, a new arsenite mineral: its description and structure determination. *Am. Mineral.* **79**, 996-1002.

GREY, I.E., MADSEN, I.C. & HARRIS, D.C. (1987): Barian tomichite, $\text{Ba}_{0.5}(\text{As}_2)_{0.5}\text{Ti}_2(\text{V}, \text{Fe})_5\text{O}_{13}(\text{OH})$, its crystal structure and relationship to derbylite and tomichite. *Am. Mineral.* **72**, 201-208.

HARRIS, D.C., HOSKINS, B.F., GREY, I.E., CRIDDLE, A.J. & STANLEY, C.J. (1989): Hemloite $(\text{As}, \text{Sb})_2(\text{Ti}, \text{V}, \text{Fe}, \text{Al})_{12}\text{O}_{23}\text{OH}$: a new mineral from the Hemlo gold deposit, Hemlo, Ontario, and its crystal structure. *Can. Mineral.* **27**, 427-440.

HÜGI, M. (1988): *Mineralogie und Petrographie der Lärcheltinzone (Monte Leone Decke, Binntal, VS)*. Diploma thesis, Mineral. Petrograph. Institute, Univ. of Bern, Bern, Switzerland.

HUSSAK, E. & PRIOR, G.T. (1897): On derbylite, a new antimonio-titanate of iron, from Tripuhy, Brazil. *Mineral. Mag.* **11**, 176-179.

KRZEMNICKI, M.S. (1996): *Mineralogical Investigations on Hydrothermal As- and REE-Bearing Minerals within the Gneisses of the Monte Leone Nappe (Binntal Region, Switzerland)*. Ph.D. thesis, Mineral. Petrograph. Institute, Univ. of Basel, Basel, Switzerland.

MELLINI, M., ORLANDI, P. & PERCHIAZZI, N. (1983): Derbylite from Buca della Vena mine, Apuan Alps, Italy. *Can. Mineral.* **21**, 513-516.

MOORE, P.B. & ARAKI, T. (1976): Derbylite, $\text{Fe}^{3+}_4\text{Ti}^{4+}_3\text{Sb}^{3+}\text{O}_{13}(\text{OH})$, a novel close-packed oxide structure. *Neues Jahrb. Mineral., Abh.* **126**, 292-303.

NICKEL, E.H. & GREY, I.E. (1979): Tomichite, a new oxide mineral from Western Australia. *Mineral. Mag.* **43**, 469-471.

STECK, A. (1987): Le massif du Simplon – réflexions sur la cinématique des nappes de gneiss. *Schweiz. Mineral. Petrogr. Mitt.* **67**, 27-45.

STRECKEISEN, A., WENK, E. & FREY, M. (1974): On steep isogradic surfaces in the Simplon area. *Contrib. Mineral. Petrol.* **47**, 81-95.

Received October 16, 1996, revised manuscript accepted July 9, 1998.

THE RESPONSE OF LUMINESCENCE IN SYNTHETIC CALCITE TO LABORATORY HEATING

ROGER A. MASON¹

Department of Earth Sciences, Memorial University of Newfoundland, St John's, Newfoundland A1B 3X5

ABSTRACT

Synthetic calcite doped with Mn and Mg has been prepared from aqueous solutions of CaCl₂ using four different methods: (1) rapid precipitation using Na₂CO₃, (2) rapid precipitation using NaHCO₃, (3) rapid precipitation using ammonium carbonate, and (4) slow precipitation from solutions in contact with ammonium carbonate vapor. Calcite prepared using methods (1) to (3) forms rhombs 1 to 4 μm across and has relatively broad XRD peaks. Calcite prepared using method (4) forms rhombs up to 1 mm across and has relatively narrow XRD peak widths. Cathodoluminescence (CL) spectra were obtained to characterize the intensity, wavelength and bandwidth of emission. Calcite prepared using methods (1) and (2) generally has lower CL intensity than compositionally similar calcite prepared using methods (3) and (4). The wavelength of emission is independent of concentration where Mn and Mg total less than approximately 0.01 atoms per formula unit, but increases at higher concentrations of these elements. The bandwidth increases with the concentrations of Mn and Mg. Calcite prepared by methods (1) to (4) was heated in CO₂ and hydrothermally in the temperature range 75 to 400°C. Calcite prepared using methods (1) to (3) usually coarsens significantly, and XRD peak widths become smaller on heating, especially in the presence of water. Little change in grain size or XRD peak widths takes place on heating calcite prepared using method (4). The intensity of CL increases as a consequence of heating. Calcite made by methods (1) and (2) shows larger relative increases in CL intensity on heating than that made by methods (3) and (4). Hydrothermal treatment promotes a greater increase in CL intensity than does heating in CO₂. The wavelength of emission increases and bandwidth decreases on heating calcite that contains more than approximately 0.01 Mn and Mg *apfu*. Where the concentration of these elements is lower, changes in wavelength and bandwidth on heating are smaller and erratic in direction. The effects of heating on CL intensity and XRD peak width are attributed to the annihilation of defects during recrystallization. Changes in the wavelength and bandwidth of CL emission on heating are attributed to local redistribution of the activator ions.

Keywords: calcite, synthesis, luminescence, recrystallization.

SOMMAIRE

Ce travail porte sur la calcite synthétique dopée avec le Mn et le Mg, et préparée à partir de solutions aqueuses de CaCl₂ selon quatre protocoles différents: (1) précipitation rapide utilisant Na₂CO₃, (2) précipitation rapide utilisant NaHCO₃, (3) précipitation rapide utilisant le carbonate d'ammonium, et (4) précipitation lente à partir de solutions en contact avec des vapeurs de carbonate d'ammonium. La calcite préparée selon les méthodes (1) à (3) se présente sous forme de rhomboèdres de 1 à 4 μm de taille, et fait preuve de réflexions relativement floues en diffraction X. La calcite préparée selon la méthode (4) se présente sous forme de rhomboèdres atteignant 1 mm de taille; elle possède des raies relativement étroites. Les spectres de cathodoluminescence (CL) ont été mesurés pour en caractériser l'intensité, la longueur d'onde et la largeur de la bande d'émission. La calcite préparée selon les méthodes (1) et (2) montre en général une intensité CL plus faible que la calcite de composition semblable, mais préparée selon les méthodes (3) et (4). La longueur d'onde de l'émission est indépendante de la concentration dans les cas où les concentrations de Mn et Mg sont inférieures à environ 0.01 atomes par unité formulaire, mais elle augmente dans les cas où la concentration de ces éléments est plus élevée. La largeur de la bande d'émission augmente avec la teneur en Mn et Mg. La calcite préparée selon les méthodes (1) à (4) a été chauffée en présence de CO₂ et en milieu hydrothermal dans un intervalle de température entre 75 et 400°C. Les grains de calcite préparée selon les méthodes (1) à (3) deviennent en général plus grossiers, et les pics de diffraction X deviennent plus étroits suite au chauffage, surtout en présence d'eau. Il y a très peu de changement en granulométrie ou en largeur des pics de diffraction suite au chauffage de la calcite préparée selon la méthode (4). L'intensité de l'émission CL augmente avec le chauffage. La calcite préparée selon les méthodes (1) et (2) fait preuve d'augmentations relatives en intensité de CL par chauffage, par rapport à celle qui a été préparée selon les méthodes (3) et (4). Le traitement hydrothermal promouvait une plus grande augmentation en intensité d'émission CL qu'un traitement en présence de CO₂. La longueur d'émission augmente et la largeur de la bande diminue suite au chauffage de la calcite qui contient plus d'environ 0.01 Mn et Mg atomes par unité formulaire. Dans les cas où la concentration de ces éléments est plus faible, les changements en longueur d'onde et en largeur de la bande d'émission suite au chauffage sont minimes et erratiques en direction. Les effets du chauffage sur l'intensité d'émission CL et sur la largeur des réflexions en diffraction X seraient dus à l'annihilation des défauts par recristallisation. Les décalages en longueur d'onde de l'émission et en largeur de la bande suite au chauffage seraient attribuables à la redistribution locale des ions activateurs.

(Traduit par la Rédaction)

Mots-clés: calcite, synthèse, luminescence, recristallisation.

¹E-mail address: rmason@sparky2.csd.mun.ca

INTRODUCTION

The major control on luminescence intensity in minerals is the presence and concentration of chemical activators (such as manganese and rare-earth elements, *REE*) and quenchers (such as iron) in the phase of interest. The minimum concentrations required to activate luminescence that is detectable by eye are known to be as low as ten to twenty parts per million (Marshall 1988, Machel *et al.* 1991), but the precise dependence of luminescence intensity on concentration of activators and quenchers is unknown. It is becoming clear, however, that trace-element abundances are not the sole control on luminescence intensity. Mason (1994, 1997) has shown that heating and radiation damage significantly influence the intensity of the cathodoluminescence (CL) signal from synthetic calcite, and that in natural calcite, heating causes changes in the wavelength and bandwidth of emission, as well as in its intensity.

These observations offer the prospect that thermally induced modifications to luminescence spectra could be used to estimate the paleotemperature of a carbonate-bearing rock. Such estimates would be valuable in the temperature region below 300°C, where phase equilibria are improbable because of kinetic constraints, and especially valuable below 200°C, where the maturation of organic matter takes place.

The prospect of a geothermometer based on CL is complicated by intersample variability in response to heating, which may be dependent on composition (Mason 1997) or on crystallinity (Mason 1994). The present study extends previous work by investigating how the luminescence signal and its response to heating depend on the crystallinity and composition of synthetic calcite with grain sizes spanning the range from micrite to sparite. In addition, the effect of heating in the presence of water (conditions similar to those that would apply during burial of sedimentary rocks) is compared with heating in the presence of CO₂.

EXPERIMENTAL METHODS

The methods of synthesis were designed to produce suites of synthetic calcite of widely differing chemistry and degree of crystal perfection (crystallinity) to be used as starting calcite in a series of heating experiments.

Synthesis

Calcite was precipitated from aqueous chlorides of Ca, Mg and Mn prepared from reagent-grade powders. The concentration of CaCl₂ was 0.1 mL, and those of MnCl₂ and MgCl₂ were adjusted to produce the desired composition of calcite.

Four different methods of precipitation were used: (1) Synthesis from manganese-bearing solutions over 7 to 10 days using ammonium carbonate vapor (ACV) as the titrant. In three experiments small quantities of Mg

were present in addition to Ca and Mn. The products of this method of synthesis are called ACV calcite; further details are given in Mason & Mariano (1990). (2) Synthesis from manganese-bearing solutions by adding Na₂CO₃ (NC) solution over a period of approximately 30 minutes (NC calcite). (3) Synthesis from manganese-bearing solutions by adding ammonium carbonate (AC) solution over a period of 10 minutes (AC calcite). (4) Synthesis from manganese- and magnesium-bearing solutions by adding sodium hydrogen carbonate (NHC) powder over a period of 10 minutes (Glover & Sippel 1967) (NHC calcite). The NC and AC syntheses were carried out at low temperature (2.5 to 6°C) to avoid coprecipitation of vaterite. The ACV and NHC syntheses were carried out at room temperature. At the conclusion of an experiment, the precipitates were washed with distilled water and dried in air.

Chemical analysis

The samples were analyzed by atomic absorption (AA) for Ca, Mn and Mg. ACV calcite was also analyzed using a Cameca Camebax SX-50 microprobe equipped with a Link Analytical eXL energy-dispersion spectrometer (EDS). The concentration of Ca was measured by EDS, and that of Mg, Fe and Mn was measured by wavelength-dispersion methods. Calcite, dolomite and rhodochrosite standards were used. The operating conditions were: accelerating voltage 15 kV, beam current 10 nA, and beam diameter 20 μm.

X-ray diffraction and scanning electron microscopy

An aliquot of each starting calcite and selected samples of heated calcite were prepared for powder X-ray diffraction (XRD) to identify crystalline phases. ACV calcite was crushed under acetone and spread on a glass slide. NC, AC and NHC calcite was of sufficiently small grain-size that only disaggregation was required for slide preparation. Selected samples were mounted with Si metal in order to measure unit-cell parameters. Data were acquired using either a Philips 1800 or a Rigaku RU-200 automated diffractometer. Samples were mounted on Al stubs and coated with gold before being examined with either a Cambridge Instruments Stereoscan 250 or a Hitachi S-570 scanning electron microscope.

Heating

Heating was carried out in the presence of CO₂ by filling a vertical ceramic-lined tube furnace with the pure gas. Temperatures were recorded every few minutes during the 15- to 20-minute warm-up period and thereafter, several times per day. Recorded temperatures did not vary by more than 3°C after warm-up and are believed to be accurate to ±5°C. Quenching to room temperature took 2 to 3 minutes.

The starting calcite was sealed in platinum tubes for experiments conducted in the presence of water (hydrothermal experiments). The amount of water added was from 0 to 8.6 wt%. The starting calcite was not dried before loading the tubes, so that adsorbed water was always present. Pressure was measured by a calibrated Bourdon gauge and transmitted by argon gas. Temperature was read every few minutes during the 20- to 40-minute warm-up time and thereafter several times per day. Recorded temperatures are accurate to within 5° and did not vary more than ± 2 to 4°C over the period of each experiment.

At the end of the experiment, the pressure vessel was cooled isobarically in a stream of compressed air. The tubes were cleaned and weighed. Those showing a weight change of more than ± 0.0005 g were considered to have leaked and were discarded.

Luminescence measurements

Luminescence was excited using a modified JEOL JXA-50A electron microprobe operating at an accelerating voltage of 10 kV with a beam diameter of approximately $50\ \mu\text{m}$ and a beam-current density of approximately $14\ \mu\text{A}/\text{mm}^2$.

Spectra were collected on a Gamma Scientific NM-3H monochromator coupled to the microprobe optics by a fiber optic cable. All other instrumental details are as in Mason (1994). Seven to ten spectra were collected from each sample. Each spectrum was corrected for photomultiplier dark current and background (see below). Comparisons between samples are based on spectra collected in the same range of wavelengths (500 to 800 nm); consequently, corrections for photomultiplier response were not applied. The wavelength scale of the monochromator was calibrated in the range 300 to 1000 nm using the emission from a mercury vapor lamp.

Each spectrum was fitted using a background function ($y = b_0 \exp[-x/b_1]$), with b_0 the amplitude and b_1 the rate), and a peak function (the Haarrhoff - Van der Linde function):

$$y = \frac{a_0 a_2 \exp\left(-\frac{1}{2} z^2\right)}{a_1 a_3 \sqrt{2\pi} \left[\exp\left(\frac{a_1 a_2}{a_2^2}\right) - 1 \right]^{-1} + \frac{1}{2} \left[1 + \operatorname{erf}\left(\frac{z}{\sqrt{2}}\right) \right] } ,$$

in which a_0 is the area, a_1 the center of the undistorted peak, a_2 the width, a_3 the distortion, and $z = (x - a_1)/a_2$. This function accommodates asymmetrical peaks. The constants derived from the fitting procedure were averaged to derive values for the CL intensity, wavelength, bandwidth and standard errors in these parameters. Throughout this work, the quoted CL intensity refers to the peak area, emission wavelength is given as the peak center (position of the maximum calculated signal, denoted λ), and bandwidth is given as the full-width at half-maximum height (Γ). The area under the peak is a better measure of intensity than is peak height because

it takes account of differences in peak width among the samples.

Measurements on starting calcite were used as a reference against which spectra from heated calcite were compared. Changes in the CL parameters following heating are measured by the intensity ratio I_H/I_{Ref} (H: heated, Ref: reference), change in emission wavelength, $\Delta\lambda = \lambda_H - \lambda_{\text{Ref}}$, (nm) and change in bandwidth, $\Delta\Gamma (= \Gamma_H - \Gamma_{\text{Ref}}$, nm).

RESULTS

Nature of the starting calcite

ACV calcite forms transparent rhombs, typically $50\ \mu\text{m}$ to $1\ \text{mm}$ on a side, in some cases with irregular terminations. ACV calcite precipitated from Mg-bearing solutions has fewer well-developed faces than that precipitated from Mg-free solutions. Vaterite was found in the products of some (Mg-free) experiments, invariably aggregated into spheres and easily removed by hand-picking before the CL measurements and heating experiments were performed.

AC and NC calcite form rhombs and modified rhombs typically less than $1\ \mu\text{m}$ across, usually aggregated into spheroidal masses (Fig. 1a) and, in some cases, with a spherulitic texture. NHC calcite with high Mn and Mg forms aggregates of modified rhombs that range from less than 1 to $4\ \mu\text{m}$ across, the larger sizes

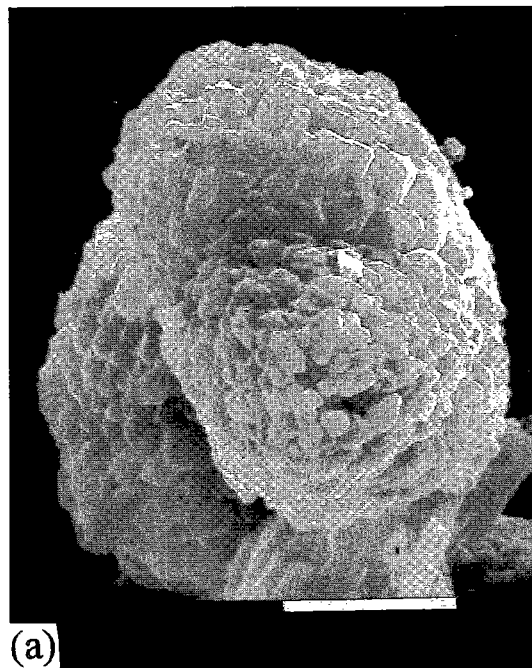


FIG. 1a. Physical appearance of NC calcite. Scale bar: $3\ \mu\text{m}$.

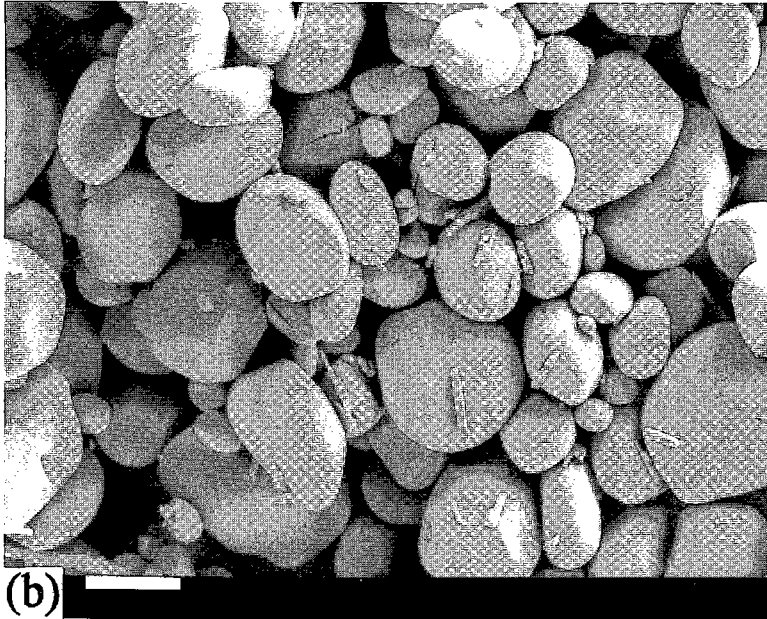


Fig. 1b. The same calcite as shown in Figure 1a after heating at 400°C for 96.7 hours in the presence of water. Note the increase in grain size and loss of edges and faces compared with (a). Scale bar: 10 μm .

being found in samples containing lower concentrations of Mn and Mg. Two samples of NHC calcite have compositions that lie inside the calcite – dolomite solvus. XRD spectra show that they are single-phase, though with broad reflections.

Table 1 gives the bulk compositions. The bulk Mn concentration for ACV calcite ranges from 1×10^{-4} to approximately 0.04 atoms per formula unit (*apfu*). Magnesium is present in three samples, attaining 0.03 *apfu*. Manganese concentrations in AC calcite range from 7×10^{-4} to 1.4×10^{-3} *apfu*. Manganese concentrations in NC calcite lie between 3×10^{-4} and approximately 0.01 *apfu*. In NHC calcite, Mn concentrations are between 0.004 and 0.09 *apfu*, and Mg reaches 0.3 *apfu*. NHC calcite with a high concentration of Mn also has high Mg. These elements total 0.33 *apfu* in two samples.

ACV calcite is zoned in Mn and, where present in the starting solution, Mg. Both sector and concentric patterns of zonation are observed. Manganese concentrations in individual CL zones range from below the limit of detection of the microprobe (6.6×10^{-4} *apfu*, 2σ) to a high of 0.07 *apfu*. Magnesium concentrations in individual zones attain 0.05 *apfu*. Calcite crystals made by the AC, NC and NHC methods are too small for microprobe analysis and for zoning to be detected.

With the exception of NHC calcite with high concentrations of Mn and Mg, the unit-cell dimensions are

very close to the values for calcite given by Reeder (1983). There are no systematic differences attributable to method of synthesis, but both *a* and *c* become shorter with increasing replacement of Ca by Mn and Mg.

Luminescence of starting calcite

The luminescence measurements are given in Table 1. Figure 2 shows the CL intensity as a function of Mn content. The data shown were collected in a single day, and great care was taken to ensure stability of the microprobe during data collection.

Intensity increases with Mn concentration to a maximum for ACV calcite containing approximately 0.04 Mn *apfu*. NHC calcite, in contrast, shows systematically declining intensity of emission between 0.004 and 0.09 *apfu* Mn. Within the composition range from approximately 0.005 to 0.04 Mn *apfu*, therefore, two different trends of concentration dependence are observed. Calcite synthesized by the NC method generally has slightly lower intensity of luminescence than compositionally similar AC and ACV calcite.

Starting calcite has emission wavelength (λ) in the range 598 to 618 nm (Table 1). There is no evidence of any dependence of λ on method of synthesis. In ACV and NHC calcite, there is a positive dependence of wavelength on the combined concentrations of Mn and Mg that becomes apparent when these elements total

TABLE 1. CHEMISTRY AND LUMINESCENCE DATA FOR STARTING CALCITE

Run	Type	Ca ⁺	Mg	Mn	I [†]	λ^{\ddagger} (nm)	Γ^{\S} (nm)
94007	AC			0.00072	10.6 (0.3)	600.1 (0.2)	78.3 (0.1)
94008	AC			0.00082	27.4 (0.3)	599.9 (0.0)	79.5 (0.0)
94009	AC			0.00147	13.8 (0.3)	600.1 (0.1)	78.7 (0.1)
88001	AC			0.00003	0.4 (0.0)	602.4 (2.6)	77.0 (3.3)
88020	AC			0.00006	2.2 (0.2)	600.0 (0.8)	78.7 (0.8)
89029	ACV	0.981	<dl	0.00013	7.4 (0.9)	599.8 (0.3)	79.0 (0.2)
89030	ACV	0.951	<dl	0.00032	5.6 (0.6)	600.6 (0.3)	78.2 (0.3)
90040	ACV	0.898	<dl	0.03560	38.9 (2.0)	605.3 (0.2)	79.4 (0.2)
90043	ACV			0.00027	6.0 (0.6)	601.5 (0.8)	81.2 (0.7)
92014	ACV			0.00892	31.4 (0.4)	600.3 (0.1)	79.2 (0.1)
92015	ACV			0.00792	26.7 (1.0)	599.3 (0.3)	79.7 (0.2)
94029	ACV	0.943	0.007	0.00018	4.6 (0.1)	602.7 (0.9)	80.6 (0.6)
94030	ACV	0.923	0.011	0.00011	6.7 (0.3)	601.6 (0.3)	81.0 (0.3)
94031	ACV	0.906	0.031	0.00018		606.5 (0.2)	81.3 (0.6)
92019(a)	NC			0.00059	4.8 (0.7)	600.7 (0.2)	79.6 (0.3)
92019(b)	NC			0.00049	1.9 (0.1)	602.1 (0.3)	76.2 (0.4)
92020(a)	NC			0.00992	27.9 (0.5)	599.9 (0.2)	80.8 (0.2)
92020(b)	NC			0.00567	16.6 (0.3)	600.2 (0.6)	78.6 (0.1)
92020(c)	NC			0.00030	3.1 (0.1)	600.5 (0.3)	78.0 (0.1)
94101	NHC	0.708	0.305	0.02952	6.9 (0.1)	610.8 (0.5)	92.4 (0.3)
94102	NHC	0.943	0.050	0.00648	15.5 (0.6)	605.4 (0.3)	81.7 (0.1)
94103	NHC	0.964	0.024	0.00747		600.6 (0.1)	81.2 (0.0)
94104	NHC	0.973	0.017	0.00431		600.3 (0.1)	80.6 (0.1)
94105	NHC	0.983	0.006	0.00361	31.2 (1.4)	602.0 (0.2)	80.6 (0.7)
94110	NHC	0.688	0.247	0.09109	2.8 (0.1)	618.0 (0.4)	92.0 (0.5)
94111	NHC	0.964	0.028	0.00458		597.8 (0.2)	84.1 (0.1)
94112	NHC	0.972	0.016	0.00624		598.5 (0.1)	81.9 (0.1)
94113	NHC	0.981	0.006	0.00523		599.5 (0.1)	79.4 (0.1)
94114	NHC	0.985	<dl	0.00624		599.6 (0.1)	79.2 (0.2)

[†] Atoms per formula unit. Analyses by atomic absorption except values in italics by microprobe, for which limits of detection are: Mg 5.3×10^{-4} atoms p. f. u.; Mn 6.6×10^{-4} atoms p. f. u. (2 σ).

[‡] Standard error in brackets

[§] Wavelength.

[¶] Full-width-at-half-maximum-height

more than approximately 0.01 *apfu* (Fig. 3). There is no discernible dependence of wavelength on composition at lower concentrations for any of the different types of starting calcite. (See the Discussion regarding the choice of total Mn and Mg as the independent variable in this and other figures.)

The range of bandwidths (Γ) observed for the synthesis products is 76 to 92 nm, but only two samples of

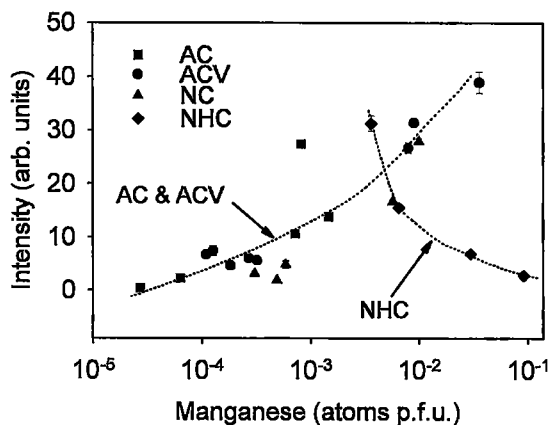


FIG. 2. Relationship between CL intensity and Mn concentration for starting calcite. The dotted lines highlight trends described in the text. Concentration is plotted on a logarithmic scale. Error bars are less than the symbol size, except where shown.

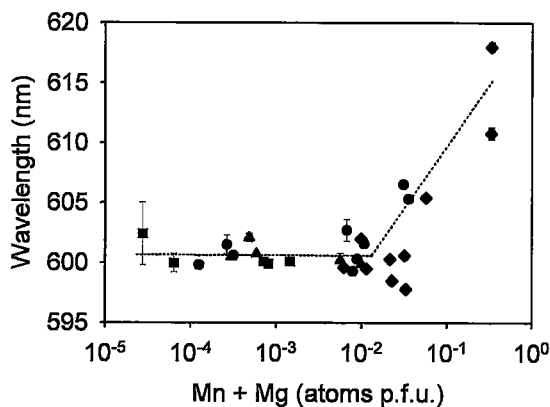


FIG. 3. Dependence of the wavelength (λ) on the combined concentration of Mn and Mg. Concentration is plotted on a logarithmic scale. Symbols as Figure 2.

starting calcite have Γ greater than 82 nm (Table 1). Bandwidth increases with the combined concentrations of Mn and Mg (Fig. 4). There is no evidence of any systematic dependence of Γ on method of synthesis.

Effects of heating on CL spectra

Heating experiments were carried out at temperatures in the range 75 to 400°C for up to 1921 hrs, with the majority of experiments in the range 15 to 50 hrs. Pressure in the hydrothermal experiments was 500 ± 40 bars except in a series of experiments on AC calcite at 300°C, in which pressures of 930, 1660 and 2146 bars were used. Pressure in the CO₂ experiments was approximately 1 bar. Results of luminescence measurements on heated calcite are presented in Table 2.

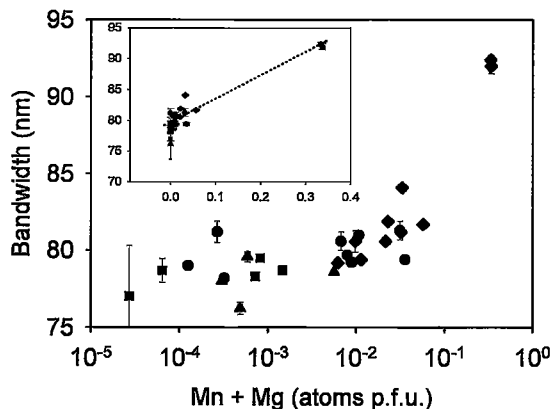


FIG. 4. Dependence of bandwidth (Γ) on the combined concentration of Mn and Mg. The apparent change in slope near 0.06 *apfu* is an artifact of the logarithmic scale used for concentration. Symbols as Figure 2.

TABLE 2. CHANGES IN LUMINESCENCE PARAMETERS FOR HEATED CALCITE

Run	Starting calcite	Temp. (°C)	Time (hours)	I_p/I_{p0} ¹	$\Delta\lambda$ (nm)	$\Delta\tau$ (nm)	Run	Starting calcite	Temp. (°C)	Time (hours)	I_p/I_{p0} ¹	$\Delta\lambda$ (nm)	$\Delta\tau$ (nm)
NC 250 °C							CO ₂ (1 bar)						
95013	92020(b)	251	4	1.81 (0.06)	-3.91 (0.23)	-0.99 (0.49)	95025-1	94008	123	28.2	1.16 (0.03)	-0.21 (0.20)	-0.02 (0.49)
95014	92020(b)	251	24.4	1.75 (0.06)	-5.96 (0.19)	-1.12 (0.49)	95061-1	94008	128	1920.8	1.14 (0.05)	-0.83 (0.36)	0.65 (0.41)
95010	92020(b)	253	71.1	1.98 (0.20)	-6.28 (1.18)	0.03 (0.95)	95027-1	94008	196	28	1.13 (0.04)	1.21 (0.34)	-0.88 (0.52)
95011	92020(b)	250	100.3	2.06 (0.21)	-5.21 (1.19)	-0.17 (0.97)	94092	94008	407	24.1	1.55 (0.04)	1.23 (0.22)	-1.48 (0.47)
95015	92020(b)	252	124.9	1.84 (0.07)	-6.90 (0.22)	-1.61 (0.48)	AC 75 - 400 °C						
95012	92020(b)	250	150	1.99 (0.25)	-3.37 (0.92)	-0.84 (0.87)	95022	94009	81	44.8	1.20 (0.05)	-0.91 (0.28)	1.26 (0.48)
NC 300 °C							95032-1	94009	70	160.4	1.13 (0.03)	-0.92 (0.15)	0.81 (0.36)
95007	92020(b)	302	24	2.09 (0.18)	-4.44 (1.07)	-1.98 (0.91)	95023-1	94009	94	42.7	1.12 (0.05)	-0.57 (0.23)	-0.41 (0.45)
95008	92020(b)	301	73.5	2.15 (0.19)	-3.92 (0.78)	-2.07 (0.86)	95024-1	94009	117	42.6	1.06 (0.02)	-0.91 (0.24)	1.73 (0.40)
95009	92020(b)	301	307.5	2.35 (0.19)	-1.62 (0.69)	-1.56 (0.78)	95021	94009	122	45	1.15 (0.02)	0.03 (0.15)	0.68 (0.38)
NC 400 °C							95020	94009	203	44.3	1.33 (0.04)	-0.45 (0.07)	0.37 (0.36)
95001	92020(b)	392	2	2.91 (0.32)	-1.17 (0.59)	-0.32 (0.92)	94093	94009	400	21.8	1.75 (0.01)	0.46 (0.09)	-0.22 (0.29)
95002	92020(b)	392	4	2.99 (0.32)	-0.71 (0.74)	-0.28 (0.92)	ACV 400 °C						
95003	92020(b)	391	6	2.81 (0.32)	-0.98 (0.59)	-0.05 (0.91)	94094	94029	398	21.4	2.70 (0.20)	0.16 (0.96)	-1.06 (0.69)
95004	92020(b)	397	12.3	2.81 (0.29)	-0.20 (0.56)	-0.20 (0.80)	94089	94029	401	24	3.06 (0.21)	0.00 (0.99)	-0.88 (0.69)
95005	92020(b)	395	18.3	2.40 (0.32)	-1.37 (0.82)	0.73 (0.81)	94095	94030	404	22.7	1.33 (0.08)	1.62 (0.53)	-0.84 (0.44)
95012	92020(b)	388	26.5	2.61 (0.09)	-0.43 (0.15)	-1.32 (0.48)	94090	94030	398	24.4	1.24 (0.06)	0.83 (0.48)	-0.37 (0.49)
95006	92020(b)	396	37.7	2.86 (0.29)	1.34 (0.91)	-1.14 (0.81)	NHC 200 & 400 °C						
NC 200 to 400 °C							94106	94101	208	14.8	4.69 (0.25)	7.44 (0.99)	-3.37 (0.73)
95070	92020(c)	196	24	1.83 (0.09)	-1.55 (0.42)	1.06 (0.67)	94108	94101	402	5.6	16.54 (0.66)	9.25 (0.76)	-1.40 (0.63)
95064	92020(c)	254	23.3	1.94 (0.07)	-1.37 (0.39)	0.43 (0.63)	94116	94102	205	19.3	2.16 (0.05)	-1.51 (0.32)	-3.15 (0.44)
95067	92020(c)	301	26	2.08 (0.07)	-1.57 (0.38)	0.43 (0.66)	94115	94103	209	19.1	1.92 (0.03)	1.48 (0.25)	-2.20 (0.25)
95013	92020(c)	383	25	3.38 (0.25)	0.11 (0.53)	-0.42 (0.86)	94109	94103	394	5.9	3.35 (0.06)	1.74 (0.21)	-1.91 (0.25)
AC 200 to 300 °C							94117	94105	200	19.5	1.73 (0.04)	1.15 (0.47)	-2.14 (0.88)
95068	94007	196	24	1.43 (0.05)	-1.80 (0.28)	0.93 (0.56)	Hydrothermal: 1.5 to 8.6 wt% added H ₂ O, pressure = 500±40 bars except where noted						
95062	94007	254	23.3	1.52 (0.07)	-0.35 (0.40)	0.12 (0.59)	ACV 75 - 400 °C						
95065	94007	301	26	1.62 (0.03)	0.21 (0.48)	-0.65 (0.57)	95092	89029	75	23	0.65 (0.05)	0.83 (0.85)	-3.03 (0.85)
95069	94009	196	24	1.24 (0.03)	-0.70 (0.31)	0.00 (0.43)	95093	89029	104	22.5	0.97 (0.07)	0.41 (0.31)	-0.42 (0.69)
95063	94009	254	23.3	1.37 (0.03)	-0.44 (0.16)	-0.40 (0.40)	95051-1	89029	195	45	2.53 (0.15)	-1.07 (0.70)	0.73 (0.67)
95066	94009	301	26	1.50 (0.03)	-0.79 (0.14)	0.08 (0.38)	95056-1	89029	303	23.7	1.65 (0.10)	1.18 (0.65)	-0.79 (0.68)
NHC 400 °C							95052-1	89029	299	27	1.78 (0.15)	2.04 (0.65)	-1.46 (0.63)
94122	94101	394	24.8	5.27 (0.21)	5.44 (0.56)	-3.72 (0.61)	95055-1	89029	404	23.2	1.86 (0.10)	1.73 (0.62)	-1.63 (0.62)
94118	94102	396	18.2	3.09 (0.07)	0.41 (0.30)	-2.09 (0.38)	ACV 75 - 400 °C						
94119	94103	396	18.2	2.62 (0.04)	1.42 (0.19)	-2.82 (0.22)	95095	89030	81	22.7	1.20 (0.07)	-2.16 (0.51)	1.62 (0.38)
94120	94104	396	18.2	3.62 (0.09)	-0.55 (0.21)	-2.26 (0.46)	95096	89030	105	21.3	1.31 (0.06)	0.66 (0.35)	-0.13 (0.31)
94121	94105	394	24.8	1.69 (0.08)	0.91 (0.45)	-2.81 (0.87)	95097	89030	149	21.2	0.72 (0.02)	1.12 (0.36)	-1.02 (0.43)
94125	94110	398	21	6.70 (0.11)	10.83 (0.42)	-5.42 (0.74)	95051-2	89030	195	45	1.68 (0.16)	-2.00 (0.41)	1.89 (0.50)
94123	94110	394	24.8	6.92 (0.13)	13.06 (0.36)	-5.93 (0.75)	95052-2	89030	299	27	2.12 (0.19)	-3.52 (0.85)	3.09 (0.59)
94126	94111	398	21	4.12 (0.14)	4.75 (0.22)	-5.43 (0.34)	95053-2	89030	403	23	1.81 (0.19)	-0.60 (0.38)	0.55 (0.42)
94127	94112	392	22	3.56 (0.16)	2.91 (0.22)	-4.07 (0.43)	ACV 75 - 400 °C						
94128	94113	392	22	2.25 (0.05)	1.06 (0.23)	-2.25 (0.36)	95098	90040	79	21.9	1.33 (0.10)	-3.43 (0.57)	0.53 (0.32)
94129	94114	392	22	2.70 (0.06)	-0.04 (0.30)	-1.60 (0.35)	95099	90040	109	22	1.44 (0.07)	-2.81 (0.31)	-0.39 (0.26)
Hydrothermal: adsorbed H ₂ O, pressure = 500±40 bars							95100	90040	154	20.9	1.28 (0.07)	-4.57 (0.38)	1.90 (0.30)
NC 100 - 400 °C							95101	90040	200	20.8	1.27 (0.07)	-1.77 (0.40)	0.32 (0.33)
95080-1	92020(b)	99	45.8	1.09 (0.04)	1.86 (0.35)	-1.82 (0.47)	95056-2	90040	303	23.7	1.86 (0.08)	-1.74 (0.38)	-0.60 (0.25)
95081-1	92020(b)	149	118.4	1.81 (0.05)	1.78 (0.20)	-2.15 (0.42)	95055-2	90040	404	23.2	2.26 (0.09)	-1.56 (0.30)	-0.69 (0.30)
95082-1	92020(b)	232	120.6	2.62 (0.10)	2.79 (0.19)	-2.54 (0.48)	ACV 75 - 400 °C						
95034-1	92020(b)	302	6.4	3.00 (0.12)	0.90 (0.26)	-1.64 (0.33)	95102	90043	77	21.5	1.17 (0.06)	0.73 (0.83)	-2.04 (0.72)
95035-1	92020(b)	299	29.2	3.77 (0.14)	0.37 (0.12)	-2.07 (0.48)	95103	90043	160	21.8	1.11 (0.05)	-0.20 (0.90)	-1.65 (0.75)
95037-1	92020(b)	401	5.7	3.77 (0.15)	0.03 (0.18)	-1.83 (0.52)	95104	90043	302	24.2	1.59 (0.11)	-1.30 (0.80)	-1.10 (0.73)
NC 75 - 400 °C							95105	90043	397	24.8	1.73 (0.13)	-1.95 (0.98)	-0.85 (0.90)
95090-1	92020(c)	77	22.5	1.23 (0.04)	-0.25 (0.41)	0.58 (0.73)	ACV 400 °C						
95047-1	92020(c)	103	23.5	1.66 (0.08)	-1.65 (0.39)	2.72 (1.05)	94082	94029	400	20.4	2.63 (0.28)	0.01 (0.97)	-1.33 (0.65)
95040-1	92020(c)	104	48.2	1.91 (0.08)	-2.68 (0.44)	1.46 (0.85)	94083	94030	403	23.8	1.39 (0.07)	2.12 (0.37)	-1.59 (0.46)
95045-1	92020(c)	99	503.1	1.81 (0.07)	0.52 (0.48)	0.19 (1.20)	94084	94031	401	21.8	3.15 (0.34)	-4.07 (0.49)	0.43 (0.78)
95091-1	92020(c)	154	23	3.42 (0.09)	-0.55 (0.37)	0.62 (0.60)	NC 100 - 400 °C						
95048-1	92020(c)	198	22.3	5.71 (0.28)	-0.79 (0.38)	1.39 (0.85)	95080-2	92020(b)	99	45.8	1.44 (0.05)	1.90 (0.26)	-2.54 (0.43)
95041-1	92020(c)	198	48.2	5.26 (0.17)	-1.32 (0.45)	0.16 (0.95)	95081-2	92020(b)	149	118.4	1.75 (0.07)	1.49 (0.18)	-2.05 (0.40)
95046-1	92020(c)	197	503.8	7.03 (0.29)	-1.19 (0.52)	2.71 (1.06)	95082-2	92020(b)	232	120.6	2.33 (0.06)	1.22 (0.23)	-1.33 (0.38)
95043-1	92020(c)	298	29.7	6.34 (0.17)	0.18 (0.40)	-2.50 (0.91)	95034-2	92020(b)	302	6.4	3.99 (0.16)	0.20 (0.20)	-1.87 (0.52)
95042-1	92020(c)	302	48.4	6.22 (0.17)	0.07 (0.40)	-1.57 (0.91)	95035-2	92020(b)	299	29.2	3.93 (0.16)	0.19 (0.18)	-2.26 (0.50)
95038-1	92020(c)	300	97.5	6.33 (0.25)	-1.16 (0.24)	-1.50 (0.56)	95037-2	92020(b)	401	5.7	3.70 (0.15)	-0.16 (0.22)	-1.79 (0.51)
95077-1	92020(c)	297	663.3	3.65 (0.09)	-1.72 (0.38)	1.54 (0.65)	95036-2	92020(b)	395	30.4	3.43 (0.18)	0.34 (0.21)	-1.87 (0.50)
95050-1	92020(c)	402	27	7.02 (0.36)	-1.57 (0.40)	1.10 (0.87)	NC 75 - 400 °C						
95044-1	92020(c)	399	48	7.29 (0.22)	-0.65 (0.42)	2.12 (1.02)	95090-2	92020(c)	77	22.5	1.27 (0.04)	1.39 (0.46)	-1.22 (0.88)
95083	92020(c)	406	70.6	5.39 (0.20)	0.64 (0.38)	-0.68 (0.79)	95040-2	92020(c)	104	48.2	1.93 (0.06)	-0.34 (0.46)	-0.81 (0.99)
95039-1	92020(c)	402	96.7	5.56 (0.26)	1.33 (0.40)	0.06 (0.63)	95045-2	92020(c)	99	503.1	2.35 (0.07)	-1.37 (0.52)	1.58 (1.11)
95076-1	92020(c)	397	663	6.07 (0.15)	0.72 (0.35)	-0.71 (0.78)	95091-2	92020(c)	154	23	3.21 (0.09)	1.42 (0.43)	-0.96 (0.79)
AC 75 - 400 °C							95041-2	92020(c)	198	48.2	4.48 (0.12)	-0.38 (0.43)	-1.25 (0.92)
95030-1	94007	75	184	1.05 (0.03)	0.39 (0.22)	0.03 (0.30)	95046-2	92020(c)	197	503.8	6.10 (0.31)	-0.60 (0.37)	0.68 (0.86)
95029-1	94007	201	27.9	1.49 (0.02)	1.10 (0.14)	-0.18 (0.18)	95043-2	92020(c)	398	28.7	7.77 (0.22)	-0.84 (0.40)	-0.06 (0.91)
95078-1	94007	196	664	1.65 (0.03)	0.50 (0.37)	-0.61 (0.52)	95042-2	92020(c)	202	48.4	6.74 (0.19)	0.22 (0.41)	-2.36 (0.90)
95087-1	94007	300	21.7	1.72 (0.02)	1.55 (0.27)	-1.71 (0.50)	95038-2	92020(c)	300	97.5	6.29 (0.27)	0.02 (0.25)	-1.06 (0.83)
95079-1	94007	299	119.8	1.65 (0.02)	0.78 (0.30)	-0.80 (0.55)	95077-2	920					

Run	Starting calcite	Temp. (°C)	Time (hours)	I_H/I_{Ref}^1	$\Delta\lambda$ (nm)	$\Delta\Gamma$ (nm)
AC 75 - 400 °C						
95033-2	94008	76	27.3	1.08 (0.02)	-0.52 (0.25)	0.26 (0.50)
95031-2	94008	76	184	1.01 (0.03)	1.35 (0.22)	-1.01 (0.43)
95026-2	94008	102	27.3	0.97 (0.02)	1.77 (0.20)	-1.21 (0.53)
95060-2	94008	99	1920.4	1.32 (0.04)	0.15 (0.38)	-0.32 (0.41)
95025-2	94008	123	28.2	1.15 (0.03)	0.99 (0.23)	-1.01 (0.49)
95061-2	94008	128	1920.8	1.23 (0.07)	1.52 (0.45)	-1.11 (0.44)
95027-2	94008	196	28	1.21 (0.08)	1.30 (0.27)	-0.61 (0.53)
94087	94008	399	23.8	1.73 (0.03)	-0.28 (0.25)	-0.37 (0.49)
AC 75 - 400 °C						
95019	94009	74	24.8	1.29 (0.02)	-2.46 (0.49)	1.76 (0.46)
95032-2	94009	70	160.4	1.18 (0.02)	-0.29 (0.10)	0.12 (0.36)
95018	94009	94	25.2	1.14 (0.01)	0.39 (0.08)	-0.25 (0.30)
95023-2	94009	94	42.7	1.19 (0.04)	-1.20 (0.23)	-0.37 (0.49)
95024-2	94009	117	42.6	1.15 (0.08)	-3.13 (0.51)	2.90 (0.34)
95017	94009	201	31	1.39 (0.03)	-0.55 (0.14)	0.56 (0.32)
95086 ²	94009	300	161.5	1.58 (0.05)	0.22 (0.11)	-0.86 (0.39)
95088 ³	94009	301	24.3	1.58 (0.04)	-0.86 (0.12)	0.24 (0.40)
95089 ⁴	94009	299	23.1	1.69 (0.04)	-0.14 (0.13)	-0.92 (0.40)
95016	94009	400	29	1.78 (0.01)	0.37 (0.07)	0.04 (0.29)
94088	94009	399	103.4	1.74 (0.04)	0.41 (0.10)	-0.57 (0.32)
ACV 400 °C						
94082	94029	400	20.4	2.63 (0.28)	0.01 (0.97)	-1.33 (0.65)
94083	94030	403	23.8	1.39 (0.07)	2.12 (0.37)	-1.59 (0.46)
94084	94031	401	21.8	3.15 (0.34)	-4.07 (0.49)	0.43 (0.78)

¹ Standard errors in brackets. ² Pressure = 930 bars. ³ Pressure = 1660 bars.
⁴ Pressure = 2146 bars

X-ray-diffraction spectra show that NHC calcite with compositions inside the calcite - dolomite solvus breaks down into two phases on heating. The XRD reflections from the exsolved phases are very wide, but the patterns match a dolomite-like phase (without superstructure reflections) and calcite. Compositions estimated from the (calibrated) positions of the 104 reflections indicate that the combined concentration of Mn and Mg in the Ca-rich phase is less than approximately 0.015 *apfu*. The relative intensities of the 104 reflections suggest that the dolomite-like phase is quantitatively dominant in all the two-phase mixtures. Other samples of NHC calcite and all samples of AC, NC and ACV calcite remain single-phase on heating.

The factors that influence the value of I_H/I_{Ref} obtained in a given experiment are temperature, method of heating and method of preparation of the starting calcite. There are also consistent differences among samples prepared by the same method. There is no evidence of a pressure effect in the hydrothermal experiments within the range 500 to 2146 bars. Changes in CL intensity are accomplished within 2 to 5 hours at 100°C and above. The few data available suggest that at a lower temperature, longer experiments are required for the changes in CL intensity to be completed. The quantity of water present in the hydrothermal experiments has no influence on the value of I_H/I_{Ref} attained at any temperature or on the rate at which changes in CL intensity take place.

Heating causes an increase in luminescence intensity, with the majority of I_H/I_{Ref} in the range 1 to 7. The full range of I_H/I_{Ref} is 0.65 to 16.5, with five experiments yielding I_H/I_{Ref} less than 1 and six giving values greater than 7. The highest I_H/I_{Ref} came from an NHC starting calcite containing 0.03 Mn and 0.3 Mg *apfu* that recrystallized hydrothermally to two phases at 400°C (Table 2).

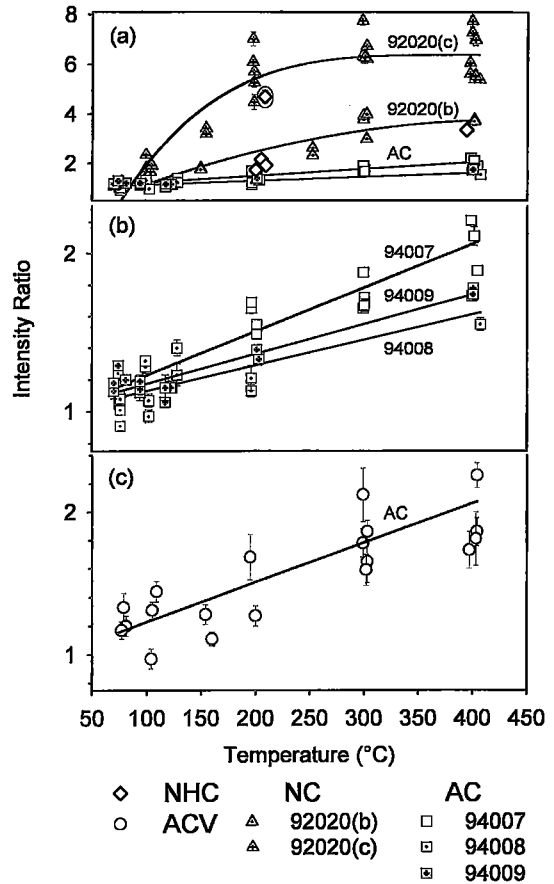


Fig. 5. I_H/I_{Ref} as a function of temperature and starting calcite for the hydrothermal experiments. Note the difference in scale of the abscissa in (a), (b) and (c). The curves and lines have no theoretical significance. The line in (c) is that for the 94007 data from (b). The circled datum on (a) is from a sample that broke down to two phases on heating. One datum for NHC calcite ($I_H/I_{Ref} = 16.5$ at 400°C) is not shown. Error bars are less than the symbol size except where shown.

The intensity ratio increases with temperature for any given starting calcite and method of heating. When heated hydrothermally, NC calcite has higher I_H/I_{Ref} at a given temperature than AC and ACV calcite (Fig. 5). The intensity ratio of heated NC calcite increases non-linearly with temperature, apparently reaching a plateau at 300 to 400°C (Fig. 5a). Intensity ratios for heated calcite 92020(b) are consistently lower than for heated calcite 92020(c). Data for hydrothermally treated NHC calcite are few, but I_H/I_{Ref} are similar to those for NC calcite (Fig. 5a). NHC calcite with compositions inside the calcite - dolomite solvus invariably broke down into two phases on heating. In general, I_H/I_{Ref} is greater for

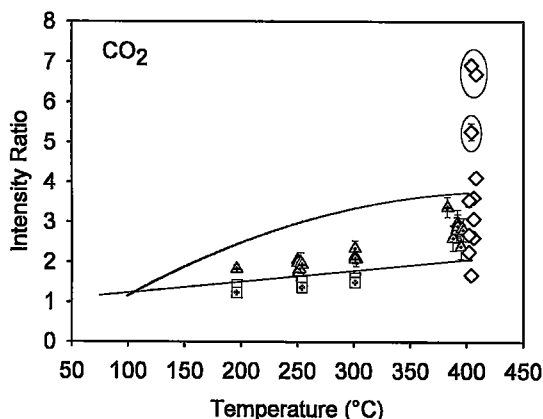


FIG. 6. Intensity ratio (I_H/I_{Ref}) as a function of temperature and starting calcite for the CO_2 experiments. The curved line is for NC calcite 92020(b) (from Fig. 5a), and the straight line is for AC calcite 94007 (from Fig. 5b). Symbols as Fig. 5. The circled data are from samples that broke down to two phases on heating.

these samples compared with NHC calcite that remains single-phase. Intensity ratios for hydrothermally heated AC calcite increase with temperature, but there is no indication that a plateau is reached over the temperature range studied. AC calcite 94007 has the highest, 94009 has intermediate, and 94008 has the lowest I_H/I_{Ref} at any temperature (Fig. 5b). Hydrothermally heated ACV calcite has intensity ratios similar to those of AC calcite heated under the same conditions; there is, however, considerable scatter in the data (Fig. 5c). There is no compelling evidence of systematic differences in I_H/I_{Ref} among samples of ACV calcite.

Heating in CO_2 generally yields lower intensity ratios than heating under hydrothermal conditions (Fig. 6). In NC calcite, the difference between the two methods of heating is relatively large, whereas in AC calcite it is small. The few data available for hydrothermal treatment of NHC calcite make clear that their I_H/I_{Ref} extend to higher values than for heating in CO_2 . There are systematic differences among the types of starting calcite, with NC calcite and NHC calcite having higher I_H/I_{Ref} than AC and ACV calcite heated under similar conditions. This behavior is similar to that observed when heating is carried out in the presence of water.

There is no significant difference in I_H/I_{Ref} between the two samples of NC calcite when heated in CO_2 . This is in contrast to hydrothermal treatment. Two samples of AC calcite heated in CO_2 differ in I_H/I_{Ref} , with calcite 94007 having consistently higher values than calcite 94009. This difference is in the same sense as observed in the hydrothermal experiments. Intensity ratios for ACV calcite heated in CO_2 (Mason 1994) are essentially the same as for hydrothermal treatment.

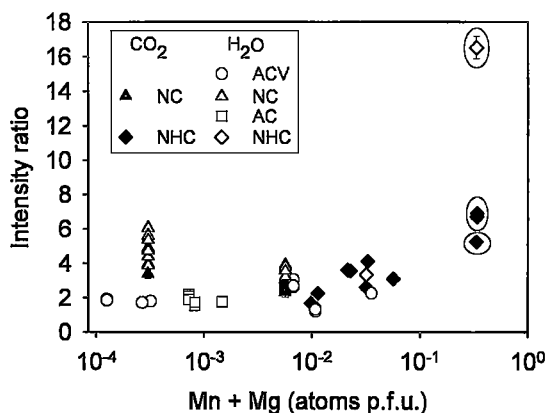


FIG. 7. Intensity ratio (I_H/I_{Ref}) as a function of the combined concentration of Mn and Mg for hydrothermal and CO_2 experiments conducted at $400^\circ C$. Concentration is plotted on a logarithmic scale. The circled data are from calcite that broke down to two phases on heating.

In heated NHC calcite, I_H/I_{Ref} increases systematically as the combined concentration of Mn and Mg increases from approximately 0.01 to 0.33 *apfu*. This trend is most clearly shown by the data for heating in CO_2 , although similar behavior is suggested by the more limited data for hydrothermal treatment (Fig. 7). The largest I_H/I_{Ref} are found for starting calcite that broke down to two phases on heating. Among heated AC, ACV and NC calcite, there is no evidence of any systematic dependence of I_H/I_{Ref} on composition, although, as described above, individual samples of NC and AC calcite attain different intensity ratios when heated under the same conditions.

An attempt was made to ascertain if I_H/I_{Ref} is a reversible function of temperature. The NC calcite 92020(c) was heated hydrothermally at $400^\circ C$ for 71 hours, resulting in an I_H/I_{Ref} of 5.4 ± 0.2 . Two portions of this heated calcite were then separated and heated hydrothermally for 164 hours at 480 bars, one portion at 100° and one at $150^\circ C$. At $100^\circ C$ there was, statistically, no change in the intensity ratio ($I_H/I_{Ref} = 5.6 \pm 0.2$), whereas at $150^\circ C$ the intensity ratio increased to 6.8 ± 0.2 . The latter value lies within the range of I_H/I_{Ref} observed for hydrothermal heating of this starting calcite at $400^\circ C$. These results show that the change in intensity induced by heating is irreversible.

Heating induced changes in the wavelength of CL emission in some experiments. The changes ($\Delta\lambda$) range from -7 to 13 nm for calcite heated in CO_2 and -4.6 to 9 nm for calcite heated hydrothermally (Table 2). In general, only changes in wavelength greater than approximately ± 1 nm are statistically significant. There was no significant change in wavelength for either of the reversal experiments.

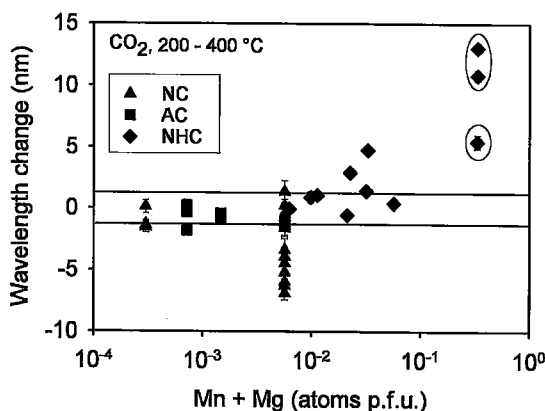


FIG. 8. Change in wavelength ($\Delta\lambda$) as a function of the combined concentration of Mn and Mg for samples heated in CO_2 at 200 to 400°C. The horizontal lines represent the approximate limits of significant change in wavelength (± 1 nm). Concentration is plotted on a logarithmic scale. The circled data are from calcite that broke down to two phases on heating.

Changes in wavelength are erratic for hydrothermally heated calcite, with no evidence that $\Delta\lambda$ is temperature-dependent. The largest $\Delta\lambda$ was recorded for heated NHC calcite (with Mn and Mg totaling 0.33 *apfu*) that separated into two phases on heating. There is no evidence of a systematic dependence of $\Delta\lambda$ on composition for the remaining samples.

Wavelength became shorter in 15 out of 19 experiments in which NC calcite was heated in CO_2 ($\Delta\lambda$ was insignificant for the remainder). There is a systematic decrease in the magnitude of $\Delta\lambda$ (from an average of -4 to -0.4 nm) with increasing temperature between 250 and 400°C. Among heated samples of NHC calcite, $\Delta\lambda$ is dominantly positive (*i.e.*, wavelength increases on heating) and increases as total Mn and Mg increases from 0.01 to 0.33 *apfu* (Fig. 8). At the latter composition, two phases formed during heating. Changes in wavelength for heated AC calcite were invariably very small.

Changes in the bandwidth ($\Delta\Gamma$) of the CL emission peak are generally small (ranging from -6 to 3.5 nm) and typically less than ± 2 nm. In hydrothermally heated NHC calcite, $\Delta\Gamma$ is consistently negative (*i.e.*, the bandwidth decreases on heating), but in AC, ACV and NC calcite, it is erratic in sign. There is no evidence of any dependence of $\Delta\Gamma$ on composition or temperature. The greatest changes in bandwidth were found in NHC calcite heated in CO_2 (Fig. 9) and, as with the hydrothermal data for this type of calcite, $\Delta\Gamma$ is consistently negative. There is no evidence of any dependence of $\Delta\Gamma$ on temperature for any of the different types of starting calcite, but Figure 9 suggests that in calcite containing more than approximately 0.01 Mn and Mg *apfu*, the CL emission band becomes narrower on heating.

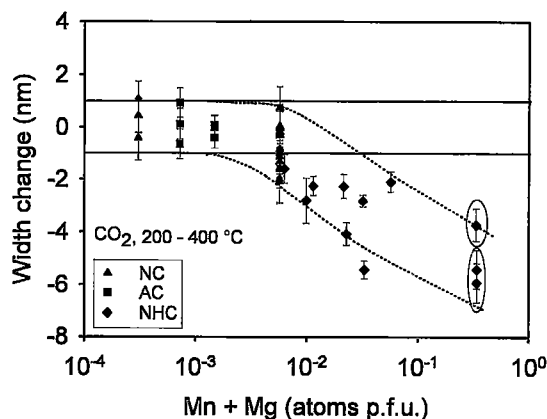


FIG. 9. Change in bandwidth ($\Delta\Gamma$) as a function of the combined concentration of Mn and Mg for samples heated in CO_2 at 200 to 400°C. The horizontal lines represent the approximate limits of significant change in bandwidth (± 1 nm). Concentration is plotted on a logarithmic scale. The circled data are from calcite that broke down to two phases on heating.

Other effects of heating

XRD peaks become narrower as a result of heating, especially under hydrothermal conditions at 300°C and above and for NC and NHC calcite. Figure 10 illustrates, for NC calcite, the spectral region containing reflections from lattice planes 214, 208 and 119. After hydrothermal treatment at 300°C or above, the width of the peaks is comparable to that of natural calcite. In contrast, heating hydrothermally at 100°C, or at any temperature in CO_2 , has little effect on XRD peak widths. AC calcite has substantially narrower XRD peaks, and heating causes only a slight reduction. In ACV calcite (Fig. 11), peak width is comparable to that of natural calcite, and heating causes no change. Notably, any decrease in the width of XRD peaks is greatest where I_H/I_{Ref} is relatively large. Unit-cell parameters did not change as a result of heating except where the starting calcite broke down into two phases.

SEM examination of heated calcite shows that there are systematic changes in grain size and morphology during heating. These are most apparent in hydrothermally heated calcite. Figure 1b illustrates an example from the NC series. After being heated hydrothermally at 400°C for 100 hours, the crystals have coarsened to 5–20 μm and have lost any faces and edges present in the starting calcite (Fig. 1a). Similar changes take place in calcite of the AC and NHC series, though coarsening of AC calcite is less extensive than that of NC calcite. Hydrothermal treatment of ACV calcite leaves the crystals essentially intact, but with a little recrystallization at the margins.

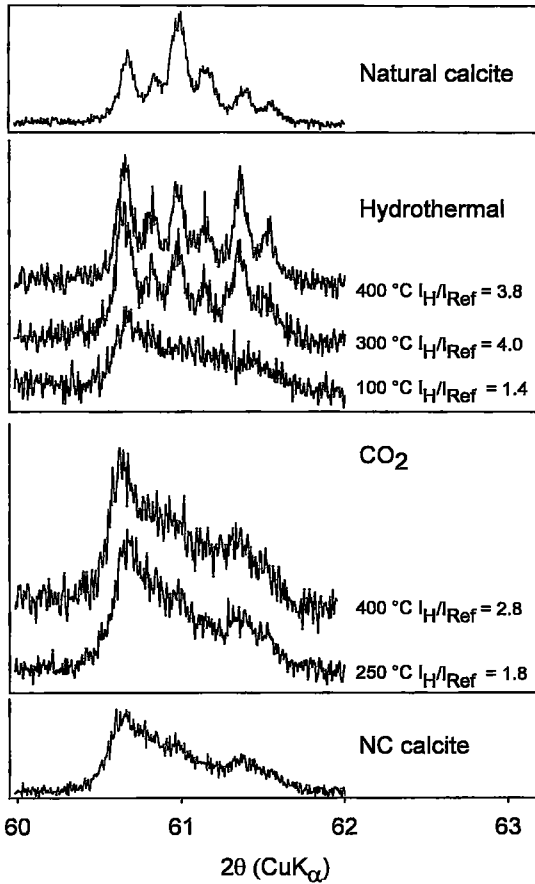


FIG. 10. XRD spectra for the 2θ region 60 to 62° for natural calcite and for AC calcite before and after heating hydrothermally and in CO_2 .

DISCUSSION

This discussion will first deal with hypotheses that may explain the data before going on to consider how the results apply to natural calcite. Finally, some comments will be presented regarding prospects for use of CL as a geothermometer.

Controls on CL intensity

The principal observations to be explained are (a) that heating of synthetic calcite causes an increase in the CL intensity, (b) that different methods of synthesis produce calcite that differs in its response to heating, and (c) that individual samples of calcite prepared by the same method differ in their response to heating. There are two hypotheses that can, in principle, explain the effect of heating on CL intensity. Both hypotheses involve changing the concentration dependence of

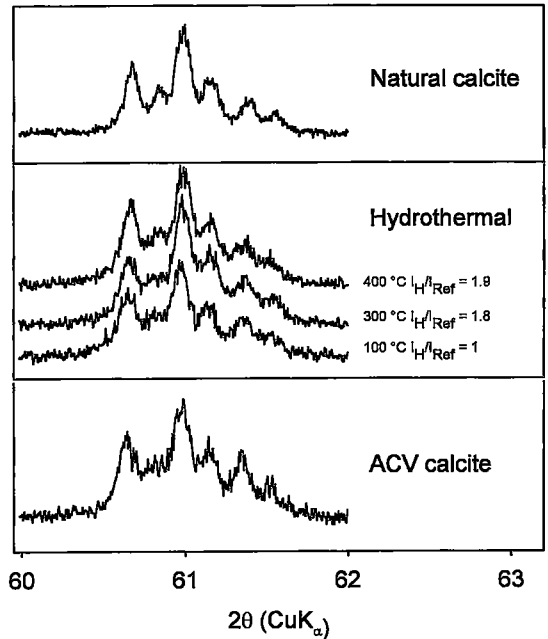


FIG. 11. XRD spectra for the 2θ region 60 to 62° for natural calcite and for ACV calcite before and after heating hydrothermally.

luminescence. A brief review of that dependence is presented below, and further details are given in Walker (1985) and Imbusch (1978). A quantitative treatment is given by Johnson and Williams (1950a, b).

As the concentration of activator ions in a matrix increases, the intensity of luminescence increases to a concentration beyond which the addition of activator ions causes it to diminish. This phenomenon (concentration quenching) arises because there is a finite probability that an activator in an excited electronic state will transfer the excitation energy to an adjacent activator that is sufficiently close. This process can continue until the excitation energy is released radiatively (*i.e.*, with the production of luminescence) or non-radiatively (*i.e.*, with the production of phonons only). Non-radiative release is more probable if the excitation energy is passed to an activator that is close to a defect (*e.g.*, a vacancy, an impurity, *etc.*) (Imbusch 1978). The more times the excitation energy is passed among adjacent activators, the greater the chance that it will eventually encounter an activator on which non-radiative decay is probable. Thus as the number of activator ions in close proximity increases, so too does the probability of non-radiative release of excitation energy.

If the distribution of activator ions on the available sites is random, then as the activator concentration is increased, the number of isolated activators will increase. So too, however, will the probability of find-

ing activators on adjacent sites in clusters of different sizes. At a high concentration of the activator, there are relatively few isolated activator ions, resulting in relatively low intensity of luminescence. The distribution of the activators on the available sites (in clusters, in random occupancy, in patterns of order, *etc.*) and the nature and concentration of defects that encourage non-radiative release of excitation energy will therefore play important roles in controlling CL intensity. The hypotheses to be considered deal with these effects; they will be stated, then compared with the evidence presented above.

The hypothesis of defects: Defects of unknown type are present at different concentrations in calcite made by different methods. Heating causes destruction of these defects, thus allowing increased CL emission without change in the bulk composition of the calcite.

The hypothesis of clusters: Calcite synthesized by different methods has differently distributed activator ions (*e.g.*, different numbers and sizes of clusters), leading to different extents of concentration quenching at a given (bulk) concentration of activator. Heating disperses the clusters, leading to enhanced efficiency of CL.

Both hypotheses explain the observations on CL intensity and its change on heating. If the hypothesis of defects is correct, then NC and NHC calcite have greater concentrations of defects than AC and ACV calcite. If the hypothesis of clusters is correct, then NC and NHC calcite have a greater portion of their Mn concentration contained in clusters than do AC and ACV calcite. The evidence from XRD spectra and from changes in the wavelength of CL emission on heating, together with indirect evidence concerning the local distribution of Mn that can be inferred from phase equilibria, are important in testing these hypotheses and will be discussed below.

XRD spectra and crystal size

As described above, both NC and NHC calcite have relatively wide XRD reflections that become significantly narrower on (hydrothermal) heating. The width of XRD reflections depends on the degree of perfection (crystallinity) of the structure and on the size of the crystals, being greater where the crystallinity is poor and crystals are small (Klug & Alexander 1974). The difference in width of XRD peaks among types of starting calcite cannot be attributed to grain-size effects because AC calcite, with relatively narrow XRD peaks, has similar grain-size to NC calcite, with wide XRD peaks. It is unlikely that the cluster hypothesis can explain differences in XRD spectra among NC, AC and ACV calcite because Mn concentrations are generally too low to cause significant structural distortion. The evidence from XRD spectra of NC, AC and ACV calcite thus favors the hypothesis of defects. The width of XRD peaks from NHC calcite with high Mn and Mg could be

explained by the distribution of these elements, by defects, or a combination of both factors.

Wavelength

The wavelength of emission depends on the number and identity of cations in the second coordination shell about an activator, because they exert an influence on the *M*-*O* distance of the activator. This changes the energy difference between the lowest excited state and the lower level state involved in emission (usually the electronic ground state) (Walker 1985, Imbush 1978). Where an activator is in dilute solution in the host, it is dominantly the host cations (Ca in the present case) that occupy the second coordination shell. As these are replaced by other substituents (Mn or Mg in the present case), the wavelength of emission should shift systematically in a direction controlled by the characteristic *M*-*O* distance of the substituent, together with any changes in distance brought about by relaxation of the structural strain associated with substitution of a differently sized ion (Waychunas 1988). Sommer (1972) demonstrated that in the rhombohedral carbonates, the wavelength of emission from Mn^{2+} increases with increasing Mg content. This is consistent with the shorter *M*-*O* distances observed in Mg-*O* polyhedra in dolomite and magnesite (Reeder 1983).

The present data do not permit the effects of Mn and Mg unambiguously to be separated because the majority of samples with substantial Mg also have a high concentration of Mn. Starting calcite lacking Mg has Mn concentrations in the range 3×10^{-5} to 0.036 *apfu* (Table 1). The starting calcite with the highest concentration of Mn in this group has the longest emission wavelength (605 nm), suggesting that wavelength increases with Mn concentration. The behavior of wavelength as a function of Mn can also be inferred from crystal-chemical arguments. In rhodochrosite, the *M*-*O* distance is 0.219 nm (Reeder 1983, Table 2a), compared with 0.210 nm for magnesite and 0.236 nm for calcite. It is expected, therefore, that the effects of Mn and Mg on λ will be complementary, substitution of both causing an increase in the wavelength of emission. This explains the systematic increase in λ that is observed for combined Mn and Mg concentrations greater than approximately 0.01 *apfu*. (This expected similarity in the effect of Mn and Mg substitution on wavelength is the reason that the total of these ions per formula unit is used as the independent variable in plots of λ and $\Delta\lambda$ as a function of composition.)

Given that local coordination controls the wavelength of emission, then changes therein must reflect changes in the coordination of the activator induced by heating. A simple interpretation based on the relations between wavelength and composition discussed above is that shifts to shorter wavelength (negative $\Delta\lambda$) reflect decreasing abundances of Mn or Mg or both around any one activator, and a positive $\Delta\lambda$ reflects an increase. In

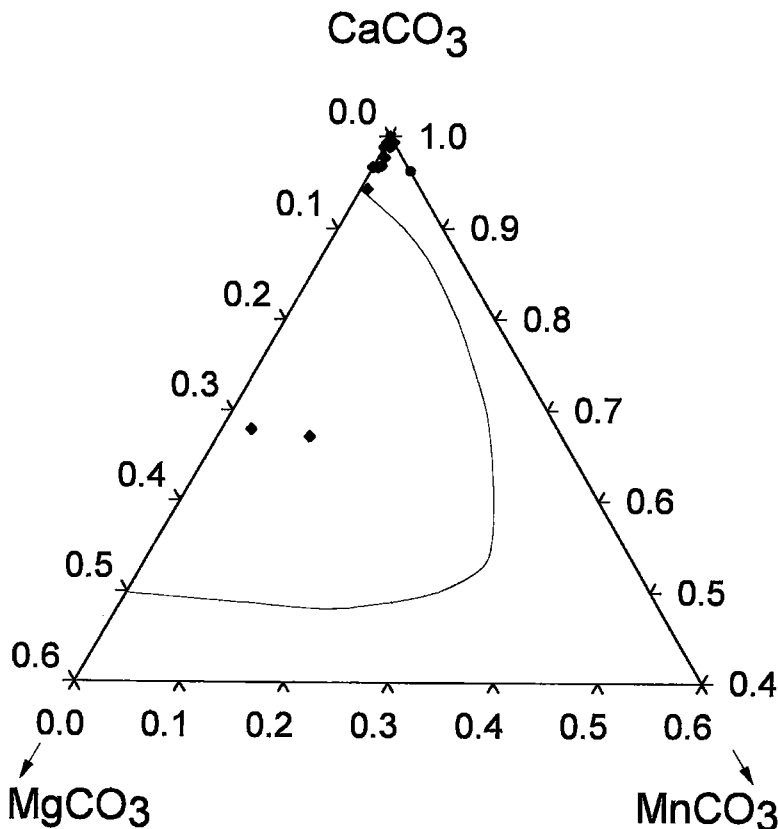


FIG. 12. A portion of the system CaCO_3 – MnCO_3 – MgCO_3 at 500°C, 10 kbar (after Goldsmith & Graf 1957). The solid symbols indicate the compositions of starting calcite. Symbols as Figure 2.

terms of the cluster hypothesis, negative $\Delta\lambda$ represents dispersal of clusters, and positive $\Delta\lambda$ represents the formation of clusters. Inferences regarding the likelihood of the formation or dispersal of clusters can be drawn from consideration of phase relations in the system CaCO_3 – MgCO_3 – MnCO_3 , together with $\Delta\lambda$.

The CaCO_3 – MgCO_3 – MnCO_3 system was studied by Goldsmith & Graf (1960). Their phase boundaries for the Ca-rich portion of the system at 500°C and 10 kbar (the closest approach to the heating temperatures used in the present study) are shown in Figure 12, along with the phase compositions of starting calcite used in the present work. In the temperature range of the present study, the ternary solvus should be slightly wider. Low pressures should also serve to widen the solvus if the data of Goldsmith & Newton (1969) on the CaCO_3 – MgCO_3 binary join extend to the ternary system. There is some uncertainty in phase relations on the join CaCO_3 – $\text{CaMn}(\text{CO}_3)_2$, the compositional region occupied by NC, AC and all but three samples of ACV calcite. Data from phase-equilibrium studies (Goldsmith

& Graf 1957, de Capitani & Peters 1981) indicate the presence of a solid solution from calcite to a composition close to Ca:Mn = 50:50, even at low temperature. However, reaction rates in this system are low, and Goldsmith (1983) and Peacor *et al.* (1987) have discussed evidence from natural assemblages suggesting that under equilibrium conditions a solvus exists between a Ca-rich solid solution and kutnohorite. If these interpretations are correct, then Ca–Ca and Mn–Mn clusters in Mg-poor calcite should be stable relative to random distributions, even for samples with compositions that lie outside the two-phase region.

Only the two samples of NHC calcite containing the greatest abundances of Mn and Mg have $\Delta\lambda$ that are large and consistent in direction between hydrothermal and CO_2 heating experiments. Manganese partitions into the Mg-rich phase in their unmixed products. This result is consistent with the observations of Lloyd *et al.* (1993) and El Ali *et al.* (1993), who have shown that in dolomite, Mn partitions into the Mg site in preference to the Ca site. The positive $\Delta\lambda$ recorded for these materials

are thus consistent with the changed coordination of Mn implied by phase separation. Partitioning of Mn into the Mg-rich phase requires slight enrichment of Mn relative to the starting calcite. This effect must lead, on average, to closer proximity of the Mn ions than in the starting calcite, and should lead to enhanced concentration quenching and a reduction in CL intensity. Instead, heating of these two samples of calcite invariably caused an increase in CL intensity. Indeed, the largest values of I_H/I_{Ref} encountered in this study came from calcite that unmixed into two phases during hydrothermal treatment. This shows that the cluster hypothesis does not explain the changes in CL intensity, at least within this range of composition.

There is no evidence of phase separation during heating of the remaining samples of NHC calcite. Although their compositions lie outside the ternary solvus (Fig. 12), at low temperature Ca-rich and Mg-rich clusters should be stable relative to a random distribution of cations, their compositions being determined by mixing properties in the Ca–Mg–Mn carbonate system. Both dispersal and growth of clusters are possible, depending on the initial distribution of cations, which is unknown. The preference of Mn for Mg-enriched carbonates (Lloyd *et al.* 1993, El Ali *et al.* 1993) makes it likely that any Mg-rich clusters will partition Mn preferentially relative to Ca-rich clusters. The predominantly positive $\Delta\lambda$ observed for these samples (when heated in CO₂) suggests that such (Mg,Mn)-enriched clusters either form or grow larger during heating. Formation or growth of Mn-enriched clusters should enhance the operation of concentration quenching and cause a reduction in CL intensity on heating. This is not the behavior observed: heating invariably causes an increase in CL intensity.

The erratic nature of wavelength changes for AC, ACV and NC calcite, which lie on the CaCO₃–CaMn(CO₃)₂ join (Fig. 12), and uncertainties regarding phase relations in this part of the system, make evaluation of the cluster hypothesis difficult for these compositions. However, if dispersal of any Mn clusters formed during crystal growth is a major cause of increased CL intensity with heat treatment, then there should be a negative relation between $\Delta\lambda$ and I_H/I_{Ref} for these materials. Such a relationship does not exist. Within the composition range of AC, ACV and NC calcite, the cluster hypothesis is unlikely to explain changes in CL intensity on heating.

Bandwidth

The bandwidth of CL depends on the extent of vibrational interaction between the activator and the ions to which it is coordinated (Walker 1985). The slight increase in bandwidth of luminescence emission with increasing concentration of Mn and Mg could be interpreted as arising solely from changes in this interaction as ions of different mass and electronic structure pro-

gressively replace Ca. If this hypothesis is correct, then the bandwidth of emission from Mn²⁺ in magnesite should differ from that in calcite. This is not the case: the bandwidth (Γ) of CL emission from magnesite is typically 77 to 85 nm (Mason, unpubl. data), a range enclosed by that of calcite in the present study.

An alternative explanation of the effect of composition on bandwidth is that increasing replacement of Ca by Mn and Mg increases the range of coordination environments of the activator. Both random substitution and chemical zoning could cause this effect (Smith 1953, Walker *et al.* 1989). If substitution of Mn and Mg is random, then simple statistics suggest that the greatest range of coordination environments of the activator should arise when Mn and Mg total 0.5 *apfu*. The present measurements are consistent with this interpretation in that Γ increases continuously up to a total Mn and Mg concentration of 0.33 *apfu*, the maximum available in this study. The critical test, to observe if Γ decreases as the total of Mn and Mg approaches 1 *apfu*, cannot be performed with the presently available data. In the absence of evidence to the contrary, it is assumed that the statistical hypothesis is correct.

Heating of NHC calcite caused the emission band to become narrower (*i.e.*, $\Delta\Gamma$ is negative). Taking the statistical hypothesis to be correct, this observation suggests that heating causes a reduction in the range of coordination environments of the activator. This interpretation is consistent with preferential partitioning of the Mn into one phase for those samples that break down into two phases on heating. It is inferred from their negative $\Delta\Gamma$ that in NHC calcite containing lesser amounts of Mn + Mg, there is an increase in clustering of these elements, but without phase separation. This inference agrees with the deductions made on the basis of changes in wavelength.

If the cluster hypothesis is correct, then dispersal of Mn-rich clusters on heating causes the CL intensity to increase. The evidence from changes in wavelength and bandwidth, together with behavior inferred from phase relations in the system CaCO₃–MgCO₃–MnCO₃, is that clusters are more likely to form or enlarge than to disperse during heating. This should lead to reduction in CL intensity, contrary to the observations. The cluster hypothesis is thus considered to be false.

Recrystallization

Morphological study by SEM shows that hydrothermal conditions are optimum for recrystallization, probably because a process of dissolution and reprecipitation can operate, whereas in CO₂ it cannot. The modest recrystallization and improvement in crystallinity that occur when calcite is heated in CO₂ suggest that the correspondingly modest increase in I_H/I_{Ref} under these conditions is a kinetic effect. Where a driving force for recrystallization exists (*e.g.*, phase separation) and a mechanism is available (*e.g.*, solution – reprecipitation),

large changes in CL intensity result from heating. Conversely, when the driving force for recrystallization is smaller, changes in CL intensity are relatively modest. It is concluded that extensive recrystallization under hydrothermal conditions aids the annihilation of defects, causing a reduction in the widths of XRD peaks and a large increase in CL intensity.

Comparison with natural calcite

Among the four methods of synthesis used in the present work, the ACV method produces calcite that is most comparable with natural calcite in terms of crystallinity (as manifested in width of XRD peaks) and of the relatively modest response of CL intensity to heating. The ACV method of synthesis is thus most appropriate if a chemically simple analogue of natural calcite is required for a study of CL. There are, nevertheless, some differences between ACV and natural calcite. The latter exhibits greater variability in the wavelength and width of the CL emission band activated by Mn^{2+} , and in the response of this band to heating (in CO_2), than does ACV calcite. Mason (1997) attributed this variability to the presence of Mg, which extends to 0.02 *apfu* compared with up to 0.03 *apfu* in ACV calcite, in addition to Mn. The present results show that the presence of Mg within this range of concentration does not explain these differences. As discussed above, the wavelength and bandwidth of CL emission, and changes in these parameters, most probably depend on the local distribution of Mn and Mg. If this interpretation is correct, differences between natural and ACV calcite may reflect greater variability in their distributions in the former. Alternatively, the presence of both Fe and Sr in natural calcite might play a role, although their low concentrations [0.004 and 0.0003 *apfu*, respectively; Mason (1997)] make this unlikely.

The existence of a temperature effect on CL intensity raises the possibility that it could be used as a geothermometer. Mason (1997) showed that whereas CL intensity in natural calcite can be modified by heating, any systematic effects are overwhelmed by variability in the response of individual samples. The present results confirm that different samples of calcite respond differently to heating. The results of attempted reversals show also that CL intensity responds in a complex way to heating at a sequence of temperatures, as might be encountered during exhumation of a sedimentary succession. The origin of these effects must be understood if the goal of using CL as a geothermometer is to be realized.

CONCLUSIONS

(1) The intensity of luminescence from synthetic calcite doped with Mn^{2+} depends on the method of preparation. Differences in CL intensity are ascribed to

differences in the density of defects acquired during crystal growth.

(2) The wavelength and bandwidth of CL of emission from calcite increase as Ca atoms are replaced by Mn and Mg.

(3) There are significant differences in the width of XRD peaks among batches of calcite synthesized by different methods. These differences are attributed to differences in the density of defects.

(4) The intensity of luminescence from Mn^{2+} -activated calcite is increased by heating, especially in the presence of H_2O . The increase is greater at higher temperatures.

(5) The magnitude of the increase in CL intensity induced by heating depends on the method by which calcite is synthesized. Differences among batches of calcite prepared by different methods are attributed to systematic differences in density of defects.

(6) Wavelength and bandwidth of CL emission may change during heating. These changes are attributed to redistribution of Mn and Mg at the available sites.

(7) XRD peaks become narrower when synthetic calcite is heated in the presence of water. The change is greatest at higher temperature and in calcite showing the largest concomitant increase in CL intensity.

(8) Individual samples prepared by the same method differ in the magnitude of their response to heating. Composition contributes to this effect, but sample-to-sample differences in density of defects also may be important.

(9) Changes in the CL intensity and reduction in XRD peak width induced by heating are attributed to annihilation of defects.

(10) Calcite precipitated from $CaCl_2$ solution by contact with ammonium carbonate vapor provides the best synthetic analogue of natural calcite in terms of its response to heating.

ACKNOWLEDGEMENTS

I thank NSERC for their support through a Research Grant. I thank Pam King and Gert Andrews, who did some of the AA analyses, Maggy Piranian for her expert assistance with the electron microprobe, and Carolyn Emerson for her help with the SEM. The hydrothermal experiments were done at the Department of Geology and Geophysics, University of Edinburgh. I thank Steve Elphic, Colin Graham and Ian Parsons for giving me access to the equipment, and the whole experimental petrology group for their help and many kindnesses. Constructive reviews by Hans Machel, Jeanne Paquette and Robert F. Martin resulted in significant improvements to the text.

REFERENCES

- DE CAPITANI, C. & PETERS, T. (1981): The solvus in the system $MnCO_3$ - $CaCO_3$. *Contrib. Mineral. Petrol.* **76**, 394-400.

- EL ALI, A., BARBIN, V., CALAS, G., CERVELLE, B. & BOUROLEC, J. (1993): Mn²⁺ activated luminescence in dolomite, calcite and magnesite – quantitative determination of manganese and site distribution by EPR and CL spectroscopy. *Chem. Geol.* **104**, 189-202.
- GLOVER, E.D. & SIPPEL, R.F. (1967): Synthesis of magnesium calcites. *Geochim. Cosmochim. Acta* **31**, 603-613.
- GOLDSMITH, J. R. (1983): Phase relations of rhombohedral carbonates. In Carbonates: Mineralogy and Chemistry (R.J. Reeder, ed.). *Rev. Mineral.* **21**, 49-76.
- _____ & GRAF, D.L. (1957): The system CaO–MnO–CO₂: solid solutions and decomposition relations. *Geochim. Cosmochim. Acta* **11**, 310-334.
- _____ & _____ (1960): Subsolidus relations in the system CaCO₃–MgCO₃–MnCO₃. *J. Geol.* **68**, 324-335.
- _____ & NEWTON, R.C. (1969): P–T–X relations in the system CaCO₃–MgCO₃ at high temperatures and pressures. *Am. J. Sci.* **267-A**, 160-190.
- IMBUSCH, G.F. (1978): Inorganic luminescence. In Luminescence Spectroscopy (M.D. Lumb, ed.). Academic Press, London, U.K. (1-92).
- JOHNSON, P.D. & WILLIAMS, F.E. (1950a): Specific magnetic susceptibilities and related properties of manganese-activated zinc-fluoride. *J. Chem. Phys.* **18**, 323-326.
- _____ & _____ (1950b): The interpretation of the dependence of luminescent efficiency on activator concentration. *J. Chem. Phys.* **18**, 1477-1483.
- KLUG, H. P. & ALEXANDER, L. E. (1974): *X-ray Diffraction Procedures for Polycrystalline and Amorphous Materials*. John Wiley & Sons, New York, N.Y.
- LLOYD, R.V., MORIE, C.S. & LUMSDEN, D.N. (1993): ESR-determined manganese partitioning ratios in dolomite synthesized at 180°C and 250°C. *Chem. Geol.* **105**, 253-257.
- MACHEL, H.G., MASON, R.A., MARIANO, A.N. & MUCCI, A. (1991): Causes and emission of luminescence in calcite and dolomite. In Luminescence Microscopy and Spectroscopy: Qualitative and Quantitative Applications (C.E. Barker & O.C. Kopp, eds.). *Soc. Econ. Paleontol. Mineral., Short Course Notes* **25**, 9-25.
- MARSHALL, D.J. (1988): *Cathodoluminescence of Geological Materials*. Unwin Hyman, Boston, Massachusetts.
- MASON, R.A. (1994): Effects of heating and prolonged electron bombardment on cathodoluminescence emission in synthetic calcite. *Chem. Geol.* **111**, 245-260.
- _____ (1997): The influence of heating on cathodoluminescence emission from natural calcite. *Can. Mineral.* **35**, 723-733.
- _____ & MARIANO, A.N. (1990): Cathodoluminescence activation in manganese-bearing and rare earth-bearing synthetic calcites. *Chem. Geol.* **88**, 191-206.
- PEACOR, D.R., ESSENE, E.J. & GAINES, A.M. (1987): Petrologic and crystal-chemical implications of cation order – disorder in kutnahorite [CaMn(CO₃)₂]. *Am. Mineral.* **72**, 319-328.
- REEDER, R.J. (1983): Crystal chemistry of the rhombohedral carbonates. In Carbonates: Mineralogy and Chemistry (R.J. Reeder, ed.). *Rev. Mineral.* **11**, 1-47.
- SMITH, A.L. (1953): Factors affecting the emission spectra of manganese-activated phosphors. *Electrochemical Soc., Spring Meet.*, 30-33 (abstr.).
- SOMMER, S.E. (1972): Cathodoluminescence of carbonates. 1. Characterization of cathodoluminescence from carbonate solid solutions. *Chem. Geol.* **9**, 257-273.
- WALKER, G. (1985): Mineralogical applications of luminescence techniques. In Chemical Bonding and Mineral Spectroscopy (F.J. Berry & D.J. Vaughan, eds.). Chapman & Hall, London, U.K. (103-140).
- _____, ABUMERE, O. E. & KAMALUDDIN, B. (1989): Luminescence spectroscopy of Mn²⁺ centres in rock-forming carbonates. *Mineral. Mag.* **53**, 201-211.
- WAYCHUNAS, G.A. (1988): Luminescence, X-ray emission and new spectroscopies. In Spectroscopic Methods in Mineralogy and Geology (F.C. Hawthorne, ed.). *Rev. Mineral.* **18**, 639-698.

Received September 9, 1997, revised manuscript accepted August 2, 1998.

APPENDIX: ERRATUM

Interested readers should note that on page 730 of Mason (1997), Figure 6 was inadvertently repeated as Figure 7. The caption to Figure 7 was printed correctly. The correct figure is reproduced below.

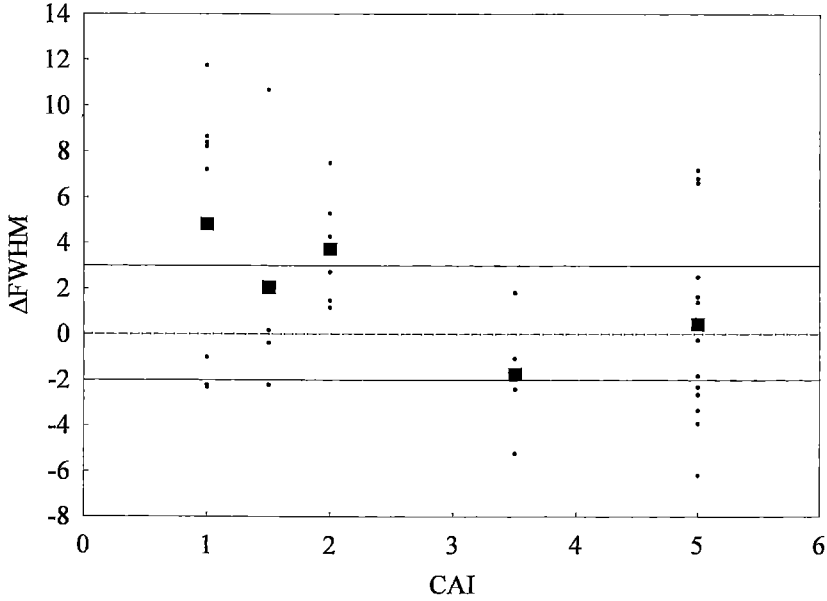


FIG. 7. Change in emission bandwidth ($\Delta FWHM$) induced by heating plotted against CAI. Mean values for each CAI group are shown as large filled symbols. The lines at -2 and +3 nm enclose the data from synthetic calcite (Mason 1994; unpubl. data).